

Starbursts in barred spiral galaxies

VI. HI observations and the K -band Tully-Fisher relation ^{*}

E. Davoust and T. Contini

UMR 5572, Observatoire Midi-Pyrénées, 14 avenue E. Belin, F-31400 Toulouse, France

Received ; accepted

Abstract. This paper is primarily a study of the effect of a bar on the neutral hydrogen (HI) content of starburst and Seyfert galaxies. We also make comparisons with a sample of “normal” galaxies and investigate how well starburst and Seyfert galaxies follow the fundamental scaling Tully-Fisher (TF) relation defined for normal galaxies. 111 Markarian (Mrk) IRAS galaxies were observed at the Nançay radiotelescope, and HI data were obtained for 80 galaxies, of which 64 are new detections. We determined the (20 and 50%) linewidths, the maximum velocity of rotation and total HI flux for each galaxy. These measurements are complemented by data from the literature to form a sample of Mrk IRAS (74% starburst, 23% Seyfert and 3% unknown) galaxies containing 105 unbarred and 113 barred ones. Barred galaxies have lower total and bias-corrected HI masses than unbarred galaxies, and this is true for both Mrk IRAS and normal galaxies. This robust result suggests that bars funnel the HI gas toward the center of the galaxy where it becomes molecular before forming new stars. The Mrk IRAS galaxies have higher bias-corrected HI masses than normal galaxies. They also show significant departures from the TF relation, both in the B and K bands. The most deviant points from the TF relation tend to have a strong far-infrared luminosity and a low oxygen abundance. These results suggest that a fraction of our Mrk IRAS galaxies are still in the process of formation, and that their neutral HI gas, partly of external origin, has not yet reached a stationary state.

Key words. Galaxies: starburst – Galaxies: active – Galaxies: evolution – Galaxies: ISM – Galaxies: kinematics and dynamics – Radio lines: galaxies

1. Introduction

The neutral hydrogen (HI) content of galaxies is a key parameter for the study of their evolution, because the HI gas is both the reservoir for future star formation and an excellent tracer of the large-scale galaxy dynamics.

It has often been suggested that the nuclear activity in galaxies is fuelled by accretion of gas toward the central regions, and that the mechanism for this radial infall is either a gravitational interaction or the presence of a bar (e.g., Noguchi 1988; Shlosman et al. 1989; Mihos & Hernquist 1994; Friedli & Benz 1993, 1995). The effect of a bar on nuclear activity has been the main motivation behind the present series of papers, and the first objective of this paper is to determine whether there is a difference in HI content between barred and unbarred galaxies.

The presence of nuclear activity should also be related to the overall gaseous content of the host galaxies, since the availability of interstellar matter is expected to affect the fueling rate of the nuclear regions. So far, only loose correlations have been found between the HI gas content and the level of star for-

mation in various samples of galaxies (e.g., Jackson et al. 1987; Mirabel & Sanders 1988; Martin et al. 1991; Eskridge & Pogge 1991; Andreani, Casoli & Gérin 1995; Contini 1996). A much tighter correlation has been found between the star formation rate (SFR) per unit area and the HI surface density in galaxies, extending over several orders of magnitudes in SFR and gas density (Kennicutt 1998). Our second objective is to investigate whether starburst and Seyfert galaxies have an abnormal neutral hydrogen content with respect to normal ones.

Another important use of HI data is for exploring the Tully-Fisher relation (Tully & Fisher 1977; hereafter TF) for active galaxies. The TF relation is an empirical correlation which predicts that the absolute magnitude of a disk galaxy is proportional to its maximum rotational velocity V_m . In spite of the frequent use of the TF relation as a distance indicator, the physical origin of this relationship is still relatively poorly understood, and it remains unclear whether all rotationally supported disk galaxies obey a single TF relation. As the fundamental scaling relation for spiral galaxies, the TF relation provides constraints on galaxy formation, because it is deeply connected to the processes by which disk galaxies form (e.g., Burstein & Sarazin 1983; Cole et al. 1994; Eisenstein & Loeb 1996; Steinmetz & Navarro 1999; Koda, Sofue & Wada 2000;

Send offprint requests to: Davoust, e-mail: davoust@obs-mip.fr

^{*} Based on observations obtained at the large radiotelescope of Observatoire de Nançay, operated by Observatoire de Paris

Navarro & Steinmetz 2000; van den Bosch 2000; Mo & Mao 2000).

Until now, the primary goal of detailed TF studies has been to establish the tightest relation possible for use as a distance indicator. Thus, most local TF studies are limited to normal isolated galaxies, excluding galaxies with nuclear activity (starburst or AGN) and with signs of interactions and/or tidal distortion (e.g., Rubin et al. 1985; Pierce & Tully 1992; Courteau 1997; Tully & Pierce 2000). The TF relation has not yet been extensively used to probe galaxy evolution. Coziol et al. (2000) have recently shown that a significant fraction of the Markarian (Mrk) starburst galaxies strongly deviate from the B -band TF relation defined for normal galaxies, suggesting that the disks of these galaxies are not in a state of dynamical equilibrium.

The third goal of this paper is to investigate whether starburst and Seyfert galaxies deviate systematically from the TF relation using K -band photometry, which is a better probe of galaxy masses than the B band. Our study complements searches for TF deviations in low-mass galaxies (Courteau & Rix 1999; O’Neil, Bothun & Schombert 2000; Hunter, Hunsberger & Roye 2000; McGaugh et al. 2000), extreme late-type galaxies (Matthews, van Driel & Gallagher 1998), asymmetric galaxies (Zaritsky & Rix 1997) and galaxies in close pairs (Barton et al. 2001).

To address the goals outlined above, we have culled a sample of galaxies from the catalogue of Markarian galaxies, retaining only those galaxies which had been detected by IRAS (in other words, those with a measured far-infrared flux).

The outline of the paper is as follows. The samples of barred and unbarred Mrk FIR-bright galaxies are described in Sect. 2. The HI observations and data reduction are presented in Sect. 3 and the results in Sect. 4. A comparative analysis of the HI content in Mrk IRAS vs. normal, and of barred vs. unbarred galaxies is given in Sect. 5.1. The behavior of Mrk IRAS galaxies in the TF plane is investigated in Sect. 5.2. Our principal conclusions are summarized and interpreted in terms of evolutionary stage of starburst galaxies in Sect. 6. Throughout this paper, all calculations assume an $\Omega = 1$ and $H_0 = 75 \text{ km s}^{-1} \text{ Mpc}^{-1}$ cosmology.

2. The two subsamples

The sample of Mrk IRAS galaxies was broken into two subsamples, barred and unbarred galaxies, according to the morphological type listed in LEDA¹.

The subsample of 144 barred galaxies contains $\sim 80\%$ of starbursts and 20% of Seyfert galaxies. It has been the subject of detailed multi-wavelength studies (Contini 1996; Contini et al. 1995, 1997a,b, 1998; Chapelon et al. 1999; Coziol et al. 1997, 1999) and is described in more details by Contini et al. (1998).

The subsample of unbarred galaxies contains 110 Mrk IRAS galaxies with nearly the same relative proportion of starburst and Seyfert galaxies as in the barred sample. It is smaller than the barred subsample, but inspection of high-resolution images of the latter subsample (Contini 1996) revealed that 15

galaxies were in fact of unbarred type, so that the two groups are in fact of comparable sizes.

3. Observations and data reduction

When a literature search for HI observations of our sample turned out a rather small number of galaxies, we decided to obtain HI observations of the Mrk IRAS galaxies that had not yet been observed.

The observations were obtained at the large decimetric radiotelescope of Nançay Observatory². The half power beam width of the telescope at 21cm is $3.6'$ (EW) $\times 22'$ (NS) at zero declination. The spectrometer is a 1024-channel autocorrelator of 6.4 MHz bandwidth, with 512 channels in each polarization. The channel resolution is 2.64 km s^{-1} at 21cm. Three runs (a total of 281 hours) were allocated for the barred subsample in 1993-94, and six runs (214 hours) for the unbarred subsample in 1996-99. We observed a total of 111 galaxies, and detected 80 (+ one companion), of which 64 are new detections.

The data were reduced at Nançay Observatory with the DAC and SIR softwares, operating on a microVax. The horizontally and vertically polarized signals were reduced separately and added after baseline subtraction. The latter operation was generally done using a polynomial of order 3. All spectra were then boxcar smoothed to a final resolution of 7.92 km s^{-1} .

There was no independent check of the absolute flux calibration; we relied on the results of Theureau et al. (1998, their Fig.4) and applied a correction of 1.12 to the fluxes obtained in the first series of runs, and of 1.32 for the second, to make up for successive changes in overall gain at zero declination and redshift. A chromatic correction was likewise applied using a series of calibrations provided by Gilles Theureau, where the temperature of the noise diode is seen to increase with decreasing frequency (increasing redshift); this correction is similar to that adopted by Thuan et al. (1999), but extends further in frequency. The gain of the antenna is 1.1 K/Jy at zero declination. A correction for loss of sensitivity with declination was done using graphs provided by the telescope staff.

The observations at a recession velocity of about 12500 km s^{-1} were considerably perturbed by radar signals, and some of the galaxy profiles around that velocity might not be reliable. In particular, we had to discard the spectra of Mrk 126, 413, 726, 1231. We also discarded the spectra of Mrk 572 and 904, because of obvious artefacts in the profiles or baselines. This leaves 106 galaxies, out of which 24 were not detected, and three (Mrk 333, 445, and UGCA 304) are not part of the sample. Mrk 445 was observed by mistake (instead of Mrk 446), Mrk 333 turned out to be undetected by IRAS, and UGCA 304 is a companion to Mrk 1337. UGCA 304 was probably not completely in the beam of the telescope, and the corresponding Nançay HI flux is thus underestimated. In summary, the total number of Mrk IRAS galaxies detected by us is 80.

In order to determine the total HI fluxes and linewidths we converted the line profiles into MIDAS tables and images and applied custom-made procedures to derive these astrophysical quantities. The total HI fluxes were corrected for beam-filling

¹ LEDA (<http://leda.univ-lyon1.fr>)

² http://www.obs-nancay.fr/html_an/a_tecrct.htm

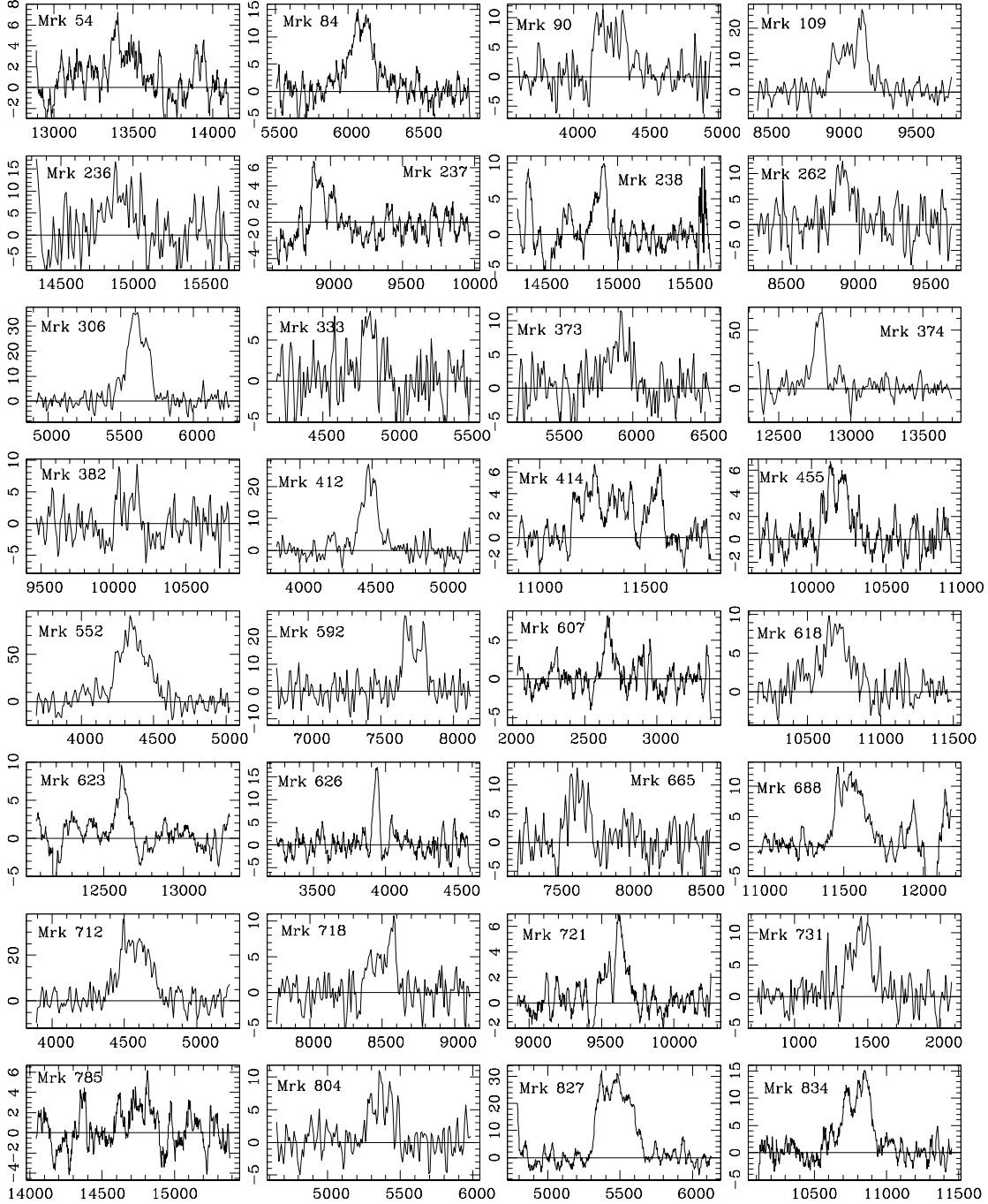


Fig. 1. HI profiles for the Mrk IRAS galaxies. The x -axis is the heliocentric velocity in km s^{-1} ; the y -axis is uncorrected flux density in mJy.

using the precepts of Theureau et al. (1998) and taking galaxy position angles and diameters in LEDA; they amount to a factor of 1.02 or less in most cases. The systemic velocity is given in the radio convention (namely $c(\nu - \nu_o)/\nu_o$). At this stage, the linewidths are corrected for cosmological stretching, but not for instrumental resolution or internal velocity dispersion. These corrections (e.g. Fouqué et al. 1990) will be applied before computing the maximum velocity of rotation.

For undetected galaxies, we determined an upper limit to the flux by measuring the rms noise and estimating the linewidth from the absolute magnitude and inclination of the galaxy via the TF relation. The HI profiles are displayed in Figs. 1 to 3.

The uncertainties in the velocities and fluxes were estimated following the method outlined in Fouqué et al. (1990).

$$\Delta V_{\odot} = 4\sqrt{RP}/SNR \quad (1)$$

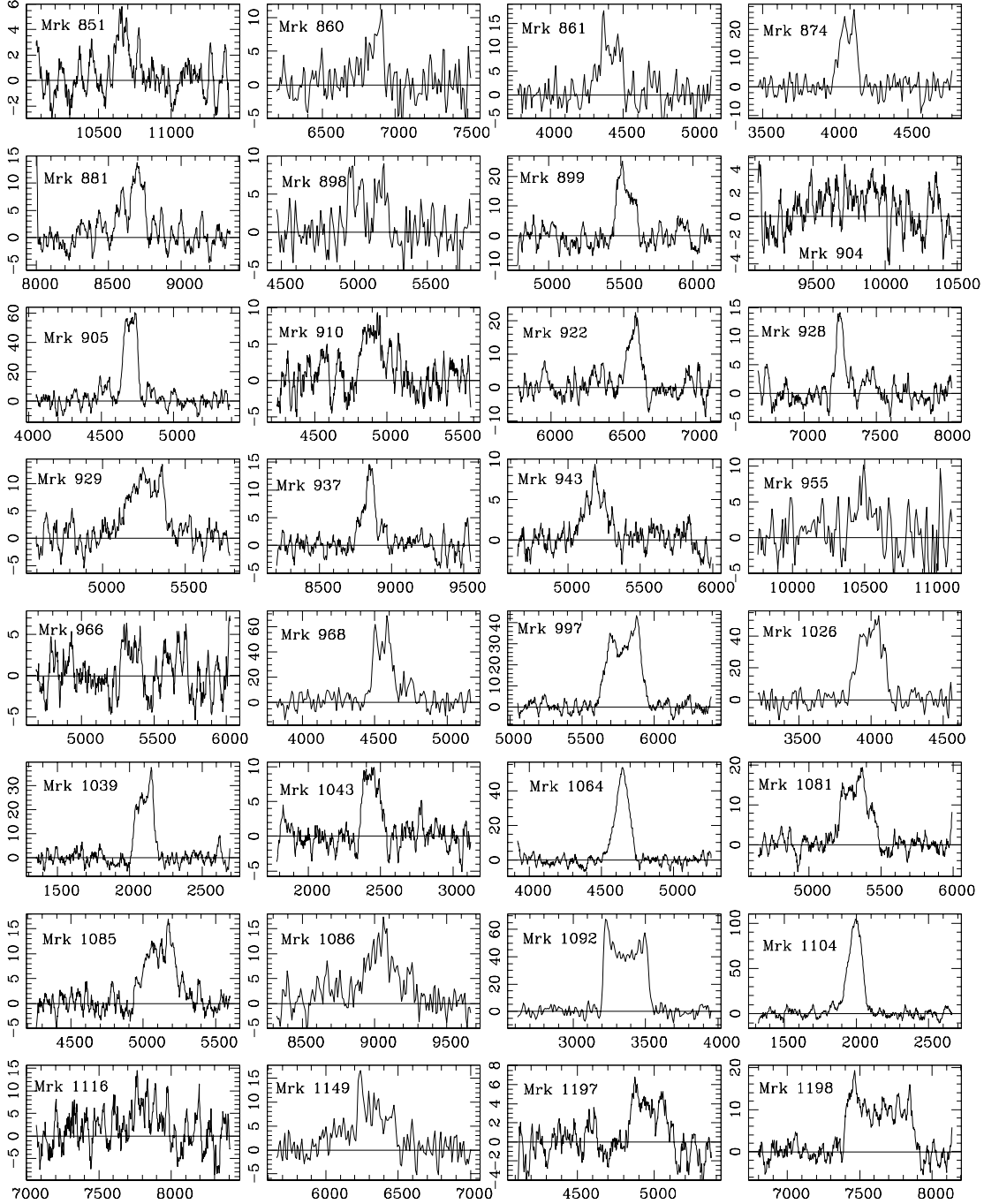


Fig. 2. HI profiles for the Mrk IRAS galaxies (*continued*).

and

$$\Delta F_{\text{HI}} = 5\sqrt{RAh}/\text{SNR} \quad (2)$$

where R is the channel resolution (identical to the channel spacing), P is the steepness of the profile (i.e. $(W_{20} - W_{50})/2$), h is the peak intensity in the profile (in Jy), A is the measured area under the profile (in Jy km s^{-1}) and SNR the signal-to-noise ratio (defined as the ratio of h to the rms noise). The uncertainties on the linewidths W_{50} and W_{20} are simply 2 and 3 times ΔV_{\odot} respectively.

4. Results

The results are presented in Table 5. The Mrk number is in col. 1, the morphological type t in col. 2, the inclination in col. 3, the radial heliocentric HI velocity (in brackets when from LEDA) and its error (in km s^{-1}) in cols. 4 and 5, the rms noise in the profile (in mJy) in col. 6, the signal-to-noise ratio (SNR) in col. 7, the measured linewidths at 20 and 50% of maximum intensity (in km s^{-1}) in cols. 8 and 9. When no line was detected, the listed W_{50} was estimated from the TF relation and

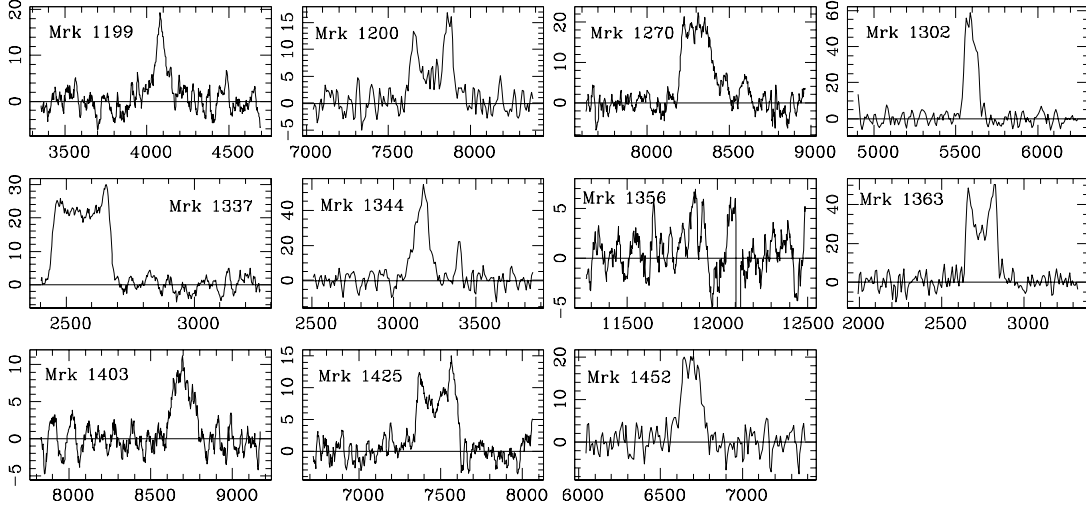


Fig. 3. HI profiles for the Mrk IRAS galaxies (*continued*).

is given in brackets. The HI flux F_{HI} (or an upper limit) and its uncertainty (in Jy km s^{-1}) are given in cols. 10 and 11. The last galaxy of that Table is UGCA 304, the companion of Mrk 1337.

The mean value of SNR (col.7) is 5.5 ± 0.3 , while the mean signal-to-noise ratio for the fluxes (col. 10) is 4.4 ± 0.3 . The uncertainty estimate for the HI fluxes is thus rather conservative.

HI data for 21 of the galaxies selected for observation appeared in the LEDA database after our observing runs were initiated. A comparison with our own data is given in Table 1. The Mrk number is in col. 1, the radial heliocentric HI velocity (in brackets when from LEDA) and its uncertainty (in km s^{-1}) in cols. 2 and 3, the measured linewidths at 20 and 50% of maximum intensity and their uncertainty (in km s^{-1}) in cols. 4 to 7. An asterisk (*) following $W20$ means that this is in fact $W25$. The maximum velocity of rotation and its uncertainty in $\log(\text{km s}^{-1})$ are given in col. 8 and 9, the HI flux F_{HI} (or an upper limit) and its uncertainty (in Jy km s^{-1}) are given in cols. 10 and 11. The signal-to-noise in col. 12 and the reference to the measurement in col 13. The references are coded as follows. 1 : this paper; 2 : Theureau et al., 1998; 3 : Giovanelli & Haynes, 1993; 4 : Haynes & Giovanelli, 1991; 5 : Henning, 1992; 6 : Davis & Seaquist, 1983; 7 : Bushouse, 1987; 8 : Giovanelli & Haynes, 1985; 9 : Andreani et al., 1995 10: Thuan et al., 1999; 11: Smoker et al., 2000; 12: Garcia et al., 1994; 13: Heckman et al., 1978; 14: Haynes et al., 1997.

The maximum velocity of rotation is defined as (Theureau et al. 1998) :

$$\log(V_M) = (2 \log(W20_c) + \log(W50_c)) / 3 - \log(2 \sin(\text{incl})) (3)$$

where $W20_c$ and $W50_c$ are the linewidths corrected for instrumental resolution and internal velocity dispersion. The upper limits to the two HI fluxes taken from the literature were re-derived using the linewidths determined by us.

The overall agreement between our data and the literature is satisfactory. The only discrepancy in the linewidths and $\log(V_m)$ concerns Mrk 1199. (Note that the discrepancy in the $\log(V_m)$ of Mrk 1200 is obviously due to the choice of inclination, which is not specified in ref. 2). The agreement among total HI fluxes is not as good, but when 3 sets of independent observations are available it appears that the fluxes of ref. 2 (Theureau et al. 1998) tend to be significantly lower than the other two. In the case of Mrk 860, the accuracy of the flux and error-bar quoted in the literature are questionable, in view of the rather short integration time. We are thus confident in the quality of our data and adopt them in all conflicting cases.

We next examine the individual profiles, taking into account the morphological type and inclinations given in Table 5. Only a few of the galaxies of our sample have the standard saddle-shaped profile: Mrk 1092, 1337, 1363, 1425 and, to a lesser extent, Mrk 90, 382, 592, 827, 898, 905, 966, 968, 997, 1200, 1270. Only one narrow profile corresponds to a nearly face-on galaxy (Mrk 626); the others (Mrk 373, 922, 928, 937, 1064, 1104) suggest that the HI may in some instances be confined to the central parts of the galaxy. Such a behavior has also been noted for the molecular gas of these starburst galaxies (Contini et al. 1997a). Conversely, some nearly face-on galaxies, like Mrk 922 and 1200, have large line widths, suggesting non-planar motions. Most profiles appear perturbed, but, because of the generally low signal-to-noise ratio, it is difficult to draw more information about the dynamics of the neutral gas from these profiles.

Finally, we note that our data on Mrk 237 might be affected by confusion, since the galaxy has a very close companion at about the same recession velocity.

5. Analysis

We complemented the HI data from our 80 galaxies by data from the literature for 138 other galaxies, to form a large sam-

Table 1. Comparison of velocities, line-widths and fluxes from our observations and the literature

Mrk	V_{\odot}	ΔV_{\odot}	W_{20}	ΔW_{20}	W_{50}	ΔW_{50}	$\log(V_M)$	$\Delta \log(V_M)$	F_{HI}	ΔF_{HI}	SNR	ref.
(1)	(2)	(3)	(4)	(5)	(6)	(7)	(8)	(9)	(10)	(11)	(12)	(13)
84	6098	18	310	54	158	36	2.119	0.120	4.30	0.99	5.0	1
84	6108	11	247	32	231	21	2.058	0.066	2.7	0.7	4.3	2
90	4253	13	264	39	221	26	2.390	0.044	2.74	0.78	4.0	1
90	4252	7	249	21	234	14	2.369	0.025	1.8	0.4	6.6	2
271	7541	23	340	69	243	46	2.339	0.088	2.41	0.74	3.4	1
271	7546		282*				2.323		1.71			7
306	5609	8	257	24	176	16	2.106	0.052	7.89	0.96	8.9	1
306	5605		246		153		2.074		5.42		30.0	3
306	5778		594*				2.554		11.90			7
359	[5043]				162				<2.19			1
359	5078		203		68		1.933	0.114	0.66		7.	3
374	12780	8	121	24	74	16	1.673	0.142	8.54	1.94	6.9	1
374									<0.29			13
382	10099	16	189	48	149	32	2.285	0.069	1.15	0.59	3.2	1
382									<0.99			13
592	7716	5	181	15	167	10	2.022	0.040	5.73	1.39	5.1	1
592	7735		250		219		2.161		4.10		7.3	4
592	7736	8			175	8	1.972		2.5	0.5		11
860	6868	10	140	30	104	20	1.811	0.129	1.50	0.52	4.6	1
860	6881	10			100	30	1.615	0.202	0.25	0.1		9
898	5072	13	296	39	256	26	2.224	0.065	1.94	0.63	4.0	1
898	5086	10	274	31	267	21	2.166	0.083	1.5	0.5	3.4	2
922	6574	10	145	30	95	20			3.18	0.99	5.4	1
922	6576		143		111				3.04	0.45	14.9	8
929	5259	16	296	48	223	32	2.232	0.078	4.43	1.04	4.3	1
929			278				2.258		3.76			8
1026	3994	8	271	24	205	16	2.221	0.040	12.87	1.59	8.2	1
1026	3989	6	260	19	212	13	2.151	0.075	7.7	0.9	11.7	2
1026	3961	15	274	45	201	30	2.221	0.075	8.3	1.9		12
1039	2111	5	161	15	134	10	1.860	0.057	6.16	0.97	8.3	1
1039	2098	65	198	17	149	11	1.940	0.623	6.76	0.40		10
1092	3356	3	338	9	311	6	2.215	0.015	19.90	1.22	14.7	1
1092	3363	4	336	13	319	9	2.174	0.020	12.2	1.3	10.8	2
1104	1991	37	155	111	109	74	2.139	0.224	16.85	4.99	1.4	1
1104	1985		135		107		2.095		21.12			5
1104			197*				2.335		14.60			6
1198	7635	10	509	30	466	20	2.414	0.032	9.63	1.79	4.9	1
1198	7647	12	511	35	495	23	2.391	0.031	3.4	0.8	4.0	2
1198									7.2	0.36		14
1199	4085	17	171	51	60	34	1.859	0.196	1.78	0.67	4.9	1
1199	4031	14	282	43	170	29	2.165	0.117	3.1	0.6	7.5	2
1200	7788	8	293	24	253	16	2.486	0.022	4.45	0.77	6.2	1
1200	7784	14	248	42	242	28	2.928	0.014	0.9	0.5	2.4	2
1270	8307	14	299	42	196	28	2.250	0.066	7.60	1.41	5.8	1
1270	8357	18	314	55	187	37	2.219	0.141	3.0	0.6	6.2	2
1363	2743	3	206	9	197	6	2.236	0.015	9.46	1.09	9.9	1
1363	2736	3	206	10	200	7	2.239	0.014	5.8	.9	10.2	2

ple of 218 Mrk IRAS galaxies, 105 unbarred and 113 barred ones, which is given in Table 7. The Mrk number is in col. 1, the morphological type (SA = unbarred, SB = barred) in col. 2, the spectral type (stb = nuclear starburst; sy = Seyfert; st? and sy? are classifications from an IRAS color index as explained below) in col. 3, the numerical morphological type t (defined in RC3; de Vaucouleurs et al. 1991) in col. 4, the inclination (in degrees) in col. 5, the isophotal diameter d_c and its uncertainty (in log of $0.1'$) in cols. 6 and 7, the maximum rotation velocity V_m (in km s^{-1}) and its uncertainty in cols. 8 and 9, the distance D (in Mpc) in col. 10, the K -band magnitude in col. 11, the oxygen abundance (O/H) with respect to solar in col. 12, the total HI mass and its uncertainty in M_{\odot} in cols. 13 and

14, the total far-infrared (FIR) luminosity (in L_{\odot}) in col. 15 and the absolute blue magnitude M_B in col. 16.

The spectral type (starburst or Seyfert) was taken from Contini et al. (1998), Mazzarella & Balzano (1986) or Mazzarella & Boroson (1993). When no classification was available, we estimated it from the IRAS color index $\alpha(60,25) = \log(S_{60}/S_{25}) / \log(25/60)$, where S_{60} and S_{25} are the IRAS fluxes at 60 and 25 μm respectively. According to Coziol et al. (1998), $\alpha(60,25)$ is larger than -1.70 for Seyferts and between -2.5 and -1.70 for starburst galaxies; this last spectral classification is of course to be taken with caution. The maximum rotation velocity $\log(V_m)$ was computed from the linewidths (given in Table 5) corrected for resolution and internal velocity dispersion (eq. 4), or taken from LEDA when not in Table 5.

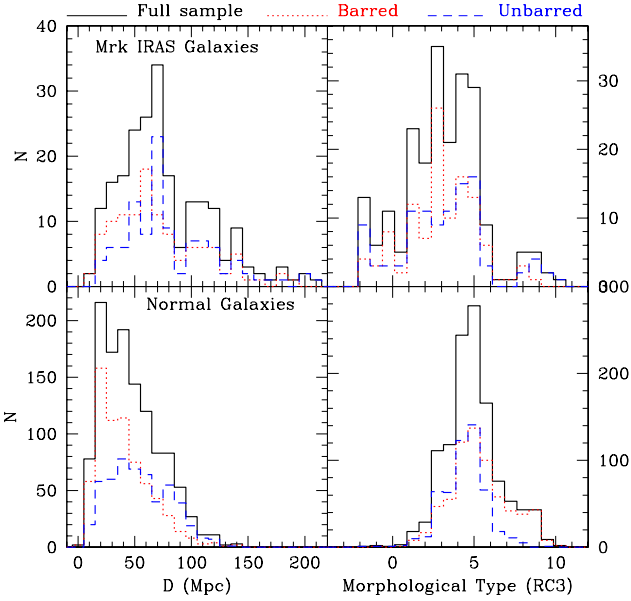


Fig. 4. Distribution of distances (*left*) and morphological types (*right*) for the sample of Mrk IRAS galaxies (*top*), and for a sample of normal galaxies from Mathewson & Ford (1996) (*bottom*). A distinction is made between barred (dotted line) and unbarred (dashed line) galaxies. The Mrk IRAS galaxies are on average further away and of earlier morphological type than the normal galaxies

The distance was estimated from the recession velocity corrected for Virgocentric flow (given in LEDA) and a Hubble constant of $75 \text{ km s}^{-1} \text{ Mpc}^{-1}$. The K -band magnitude was taken from NED³ or from Bergougnan et al. (paper VII, in preparation). The oxygen abundance was taken from Contini (1996) for the barred (SB) galaxies and from the literature, mainly Balzano (1983) and Dahari & De Robertis (1988), for the unbarred (SA) ones. The O/H for the SA are generally based on photographic work and thus more uncertain than that for the SB. The total HI mass was derived from the corrected total fluxes (given in Table 1) according to the following equation (Haynes & Giovanelli 1984):

$$\log(M_{\text{HI}}) = 5.373 + 2 \log(D) + \log(F_{\text{HI}}) \quad (4)$$

For galaxies not observed at Nançay, it was estimated from the $m21_c$ parameter in LEDA using the equation :

$$\log(M_{\text{HI}}) = 12.335 + 2 \log(D) - 0.4m21_c \quad (5)$$

The morphological type, inclination, isophotal diameter, FIR luminosity and absolute magnitude were taken from LEDA.

5.1. Neutral hydrogen content

The first questions to address are *i*) whether Mrk IRAS galaxies have an abnormal neutral hydrogen content with respect to

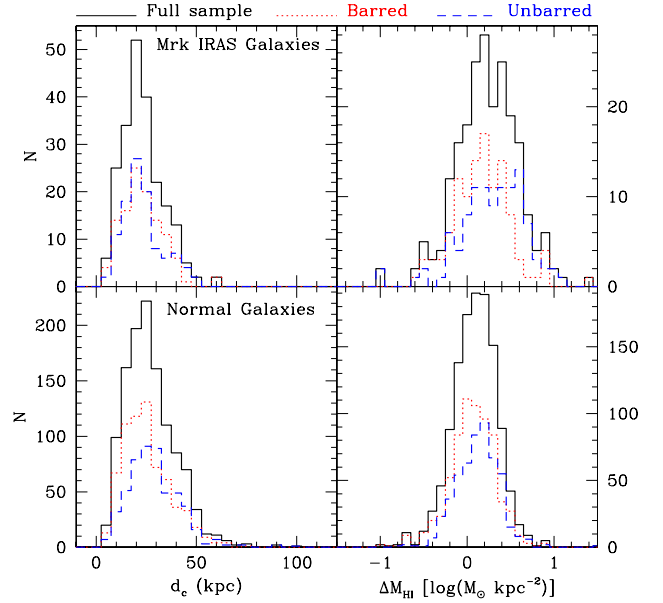


Fig. 5. Distribution of isophotal linear diameters (*left*) and excess of (*right*) HI mass for the sample of Mrk IRAS galaxies (*top*), and for a sample of normal galaxies from Mathewson & Ford (1996) (*bottom*). A distinction is made between barred (dotted line) and unbarred (dashed line) galaxies. The Mrk IRAS galaxies have on average a larger HI mass excess than the normal ones. The barred galaxies have on average a smaller HI mass excess than the unbarred ones; this is a property of spiral galaxies in general

normal galaxies, and *ii*) whether the HI content of barred and unbarred galaxies differ. As comparison sample of “normal” galaxies, we used the the sample of Mathewson & Ford (1996). In order to compare homogeneous sets of data, we only selected the 1197 normal galaxies for which the maximum velocity and HI flux were available in LEDA.

The Mrk IRAS galaxies have on average the same quantity of HI mass as the normal galaxies (see Table 2). However, this result is probably affected by selection effects. Indeed, our sample of Mrk IRAS galaxies and that of normal galaxies do not have the same distributions in distance, nor in morphological type (see Fig. 4); the Mrk IRAS galaxies are further away and of earlier type than the normal galaxies. Galaxies observed further away tend to have higher masses because of the Malmquist bias, and later-type galaxies tend to be richer in HI.

In order to circumvent the distance bias, we normalize the HI mass by d_c (the corrected linear diameter at the isophote 25 blue mag arcsec⁻²) squared, which is free of Malmquist bias. This has the dimension of an HI surface density; but one has to keep in mind that the blue isophotal diameter does not necessarily measure the radial extent of the HI distribution. The distribution of isophotal diameters d_c is shown in Fig. 5, for the sample of Mrk IRAS galaxies and for the comparison sample of normal galaxies. Mean values of isophotal diameters and HI surface densities, M_{HI}/d_c^2 , with uncertainties are listed in

³ NED (<http://nedwww.ipac.caltech.edu>)

Table 2. Mean values and uncertainties of the morphological type t , distance D , linear diameter d_c , HI mass M_{HI} , HI mass to blue light ratio $M_{\text{HI}}/L_{\text{B}}$, HI mass density M_{HI}/d_c^2 and HI mass excess ΔM_{HI} , for the sample of Mrk IRAS galaxies and for the comparison sample of normal galaxies (Mathewson & Ford 1996).

Sample	N	t	D [Mpc]	d_c [kpc]	$\log(M_{\text{HI}})$ [log(M_{\odot})]	$\log(M_{\text{HI}}/L_{\text{B}})$ [log($M_{\odot}L_{\odot}^{-1}$)]	$\log(M_{\text{HI}}/d_c^2)$ [log($M_{\odot}\text{kpc}^{-2}$)]	ΔM_{HI} [log($M_{\odot}\text{kpc}^{-2}$)]
<i>Mrk IRAS Galaxies</i>								
All	218	3.08±0.17	76.6±2.8	23.3±0.7	9.69±0.03	-0.63±0.03	7.04±0.03	0.24±0.03 ($N=199$)
Barred	113	3.04±0.21	71.9±3.7	23.5±1.0	9.65±0.04	-0.65±0.03	6.99±0.04	0.20±0.03 ($N=106$)
Unbarred	105	3.13±0.27	81.7±4.0	23.1±1.0	9.73±0.04	-0.60±0.03	7.09±0.04	0.29±0.04 ($N=93$)
<i>Normal Galaxies (Mathewson & Ford 1996)</i>								
All	1197	4.92±0.05	46.5±0.7	27.0±0.4	9.70±0.01	-0.52±0.01	6.93±0.01	0.10±0.01 ($N=1194$)
Barred	678	5.31±0.07	40.5±0.9	25.3±0.5	9.62±0.02	-0.54±0.01	6.91±0.01	0.07±0.01 ($N=677$)
Unbarred	519	4.41±0.06	54.2±1.2	29.2±0.6	9.80±0.02	-0.50±0.02	6.95±0.01	0.13±0.01 ($N=517$)

Table 2, where a distinction is made between barred and unbarred galaxies.

We find that, on average, the Mrk IRAS have a higher surface density than the normal galaxies. But, as noted above, the two samples do not have the same distributions in morphological types, which introduces another bias. To take these differences into account, we calculate the excess HI mass over that predicted for a given morphological type and diameter (d_c , in kpc), using the following equation :

$$\Delta M_{\text{HI}} = \log(M_{\text{HI}}) - c_1 - c_2 \log(d_c^2) \quad (6)$$

where the constants c_1 and c_2 are given in Table V of Haynes & Giovanelli (1984) for the different morphological types, except those earlier than S0 ($t = -1.5$). The values of excess HI mass for the different subsamples are listed in Table 2, together with the number of objects (since types earlier than S0 were not included). As a check, we corrected the HI surface densities in another way, using as reference the mean HI surface densities given by Giovanelli & Haynes (1988; their Table 12.1); this method leads to results that are in qualitative agreement with those obtained by the method of Haynes & Giovanelli (1984).

We find that Mrk IRAS galaxies have a larger excess (ΔM_{HI}) of HI mass than normal galaxies. The fact that most galaxies have a positive excess of HI mass is due to the definition of the diameter: Haynes & Giovanelli (1984) use the uncorrected diameter from UGC, whereas we use the corrected diameter from LEDA, and the LEDA uncorrected angular diameters are on average 9% smaller than the UGC diameters (Paturel et al. 1991).

We also computed the HI mass to blue light ratio for the two samples, and find that the Mrk IRAS galaxies have a lower ratio than the normal galaxies. This is contrary to expectations, and probably due to the fact that the two samples have different distributions in type (see Fig. 4) : the Mrk IRAS are of earlier type, thus of brighter absolute magnitude (see Roberts & Haynes 1994) than the other sample. There is in fact a small magnitude dependence in the HI mass to blue luminosity ratio expressed as L_{B}^{β} (see Smoker et al. 2000 and references therein). We find that $\beta = -0.33$ for both our samples. Computing $M_{\text{HI}}L_{\text{B}}^{-0.66}$ reduces, but does not reverse the trend. But this is perhaps not

Table 3. Kolmogorov-Smirnov test on the significance of the differences between samples for various parameters. The first three parameters are tested in logarithms. The numbers are confidence levels (in percent) that the two samples are drawn for different populations.

Sample	Parameter			
	M_{HI}	$M_{\text{HI}}/L_{\text{B}}$	M_{HI}/d_c^2	ΔM_{HI}
Mrk vs Normal	46.8	99.9	99.9	99.8
Mrk : SA vs SB	90.7	69.6	95.5	99.1
Normal : SA vs SB	99.9	97.0	98.0	99.9

a very good HI mass indicator, since the exponent β depends on the sample, and ranges from -0.1 to -0.33 .

We finally computed the excess HI mass over that predicted for a given morphological type and luminosity, using the constants given in Table V of Haynes & Giovanelli (1984). For this type of bias correction we find the expected trend, that the Mrk IRAS galaxies have on average a larger HI mass excess than the normal galaxies, and that the normal barred galaxies have less excess than the normal unbarred galaxies (there is no significant difference between the barred and unbarred Mrk IRAS galaxies in that respect).

These last results weaken our claim that the Mrk IRAS galaxies have more HI than normal galaxies. However, as stated by Haynes & Giovanelli (1984), normalizing the HI mass by the luminosity leads to HI mass indicators of inferior quality compared to M_{HI}/d_c^2 .

The answer to the second question, whether barred and unbarred galaxies have different HI content, is perhaps easier to give, since the detection of a bar is less likely to be biased. One could argue that bars are less conspicuous in more distant galaxies (and, indeed, the unbarred galaxies tend to be further away than the barred ones in Table 2), but our classification (in the Mrk IRAS sample) is based on high resolution images (Contini, 1996), thus less affected by the Malmquist effect.

We find that barred galaxies have on average a lower HI mass, lower HI mass to blue luminosity, lower HI surface den-

sity and lower HI mass excess than unbarred ones (see Table 2), and this is true for both Mrk IRAS and normal galaxies.

We performed Kolmogorov-Smirnov tests to quantify the statistical significance of the differences found between samples. The results are summarized in Table 3, which gives the confidence level (in percent) at which the two samples are drawn for different populations. The difference in the parameters $\log(M_{\text{HI}}/d_c^2)$ and ΔM_{HI} is significant at a confidence level of at least 95%, and mostly of 98-99%. As stated above, the significance of the differences in $\log(M_{\text{HI}})$ is probably illusory in view of possible Malmquist bias.

In summary, the two main results of this subsection are that *i*) Mrk IRAS galaxies have a larger excess of HI mass than normal galaxies, and *ii*), within each category (Mrk IRAS or normal), unbarred galaxies have a larger HI mass, mass density and mass excess than barred ones. This is a clear indication that activity (starbursts or Seyfert) and the presence of a bar are both related to the HI content of galaxies.

Finally, we must point out that we did not find any dependence of the HI mass excess on the global star formation rate of galaxies, measured by the FIR luminosity. This also holds for barred and unbarred galaxies considered separately, and by excluding Seyferts and uncertain types of nuclear activity (st?, sy?; see Table 7). On the other hand, we do find the correlation between star formation rate and HI surface density which has been established for different samples of nearby galaxies (e.g. Kennicutt 1989; Donas et al. 1990; Deharveng et al. 1994; Boselli 1994; Kennicutt 1998).

5.2. Tully-Fisher relation

The Tully-Fisher relation is one of the most basic relations among spiral galaxies and provides a critical constraint on galaxy formation theories. The third objective of this analysis is to examine whether the Mrk IRAS galaxies follow the TF relation.

We determined a TF relation for normal galaxies in the *B* and *K* bands using the sample of Mathewson & Ford (1996), extracting the relevant parameters from LEDA and NED, and restricting our analysis to galaxies with an uncertainty smaller than 0.1 on $\log(V_m)$ and an inclination larger than 30° . There were 1162 such galaxies for calibrating the *B*-band TF relation, and 682 for the *K* band. The advantage of determining our own relations, rather than relying on relations from the literature, is that we are comparing homogeneous sets of data, affected in the same way by systematic effects and errors.

In the *B* band, the relation is :

$$\log(V_m) = -0.126M_B - 0.388 \quad (7)$$

In the *K* band, it is :

$$\log(V_m) = -0.090M_K + 0.137 \quad (8)$$

The *B*-band TF relation for our sample of Mrk IRAS galaxies is shown in Fig. 6, together with the linear relation for normal galaxies. This Figure is limited to data with an uncertainty in $\log(V_m)$ smaller than 0.1 and inclinations larger than 30° . This plot shows that there is no difference between the barred

Table 4. Galaxies with the strongest deviations from the *K*-band TF relation, grouped into barred and unbarred types. The excess of HI mass (see sect. 5.1) is given in col. 5. The difference between the observed V_m and that given by Eq. 8 is in col. 6. The last column gives informations on the environment and on the level of interaction of galaxies (from Contini 1996; Keel & van Soest 1992).

Mrk	Spe	O/H	L_{FIR}	ΔM_{HI}	$\delta \log(V_m)$	Envir.
(1)	(2)	(3)	(4)	(5)	(6)	(7)
<i>Barred Galaxies</i>						
52	stb	0.78	9.72	-0.14	-0.431	isolated
300	stb	0.74	10.45	0.25	-0.350	satellite
307	stb	1.00	10.26	0.22	-0.287	isolated
313	sy2		9.55	0.87	-0.261	in group
319	stb	0.44	10.88	0.13	-0.295	pair (1.5')
353	stb	0.55	10.35	0.11	-0.342	isolated
471	sy2		10.40	0.02	-0.269	isolated
489	stb	0.57	10.74	0.91	-0.332	isolated
592	stb		10.36	0.38	-0.233	isolated
691	stb	1.50	10.12	0.45	-0.244	satellite
1157	sy2		10.05	-0.07	-0.203	isolated
1302	stb	0.90	9.68	0.41	-0.535	isolated
mean			10.21	0.30		
<i>Unbarred Galaxies</i>						
201	stb	0.44	10.59	-0.11	-0.458	merger?
331	st?		11.08	0.65	-0.239	pair (2.0')
685	st?	0.22	9.65	0.55	-0.265	isolated
905	st?		9.95	0.69	-0.442	pair (1.7')
1003	sy?		9.36	-0.12	-0.218	isolated
mean			10.13	0.33		

and unbarred galaxies. More remarkably, it also shows that the Mrk IRAS galaxies do not follow the local *B*-band TF relation, as already stated in Coziol et al. (2000), showing a large scatter.

One could argue that the luminosity in the *B*-band is dominated by young OB stars in starbursts or by the non-thermal nucleus in Seyferts and thus is not a good tracer of the total virial mass. A starburst generally brightens the galaxy by up to 2 mag in *B*, and only 0.5 mag in *K* (Mouhcine & Lançon 2003). However, there is admittedly no significant excess of galaxies with low $\log(V_m)$ compared to high- $\log(V_m)$ ones, which is surprising. One could perhaps argue that the *B*-band TF relation estimated from normal galaxies is affected by unidentified starburst galaxies in the sample, or that OB stars and dust play in opposite senses in starburst galaxies, contributing to the observed scatter. At any rate, to avoid potential problems of the *B* band, we use the *K*-band absolute magnitude as mass indicator.

The *K*-band TF relation for our sample of starburst and Seyfert galaxies is shown in Fig. 6, together with the linear relation for normal galaxies. This Figure is limited to data with an uncertainty in $\log(V_m)$ smaller than 0.1 and an inclination larger than 30° . Like the TF relation in the *B* band, we find no difference between the barred and unbarred galaxies, and a significant proportion of galaxies with very low V_m .

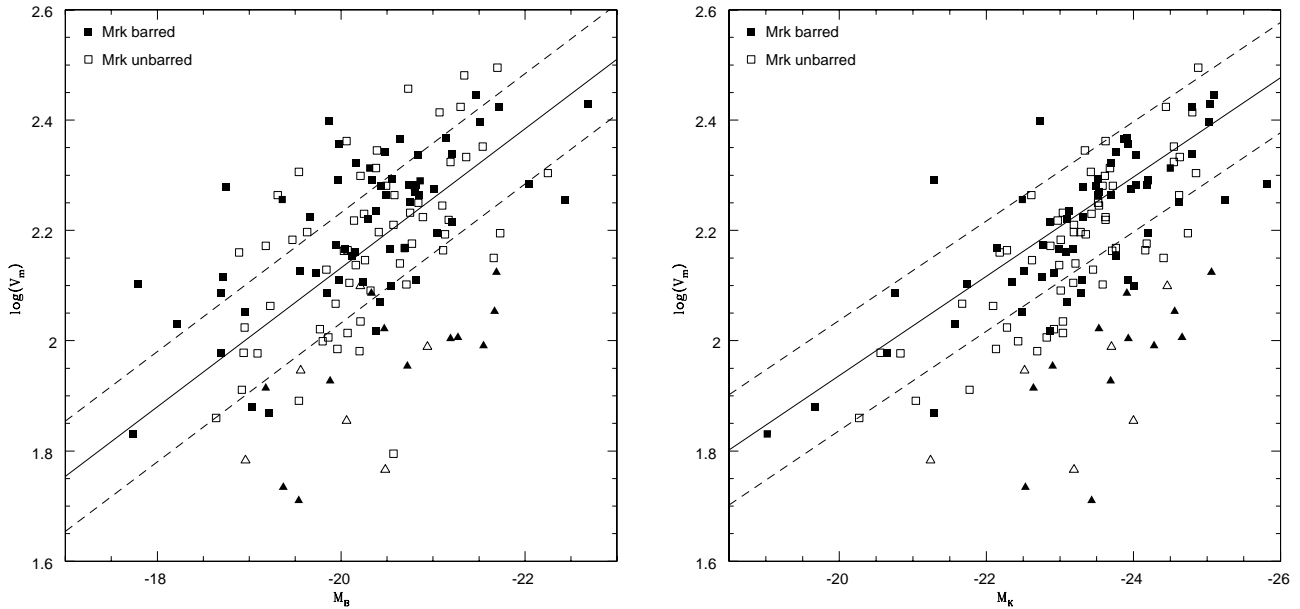


Fig. 6. Tully-Fisher relation in the B band (*left*) and in the K band (*right*) for our sample of Mrk IRAS galaxies. The full and empty squares are the barred and unbarred galaxies respectively. The full and empty triangles are the barred and unbarred galaxies which deviate most from the TF relation in the K band. These Figures are limited to data with an uncertainty in $\log(V_m)$ smaller than 0.1 and an inclination larger than 30° . The solid lines are the relation for normal galaxies (Eqs. 7 and 8). The dashed lines delineate the zone where the data should in principle be enclosed (uncertainty on $\log(V_m)$ less than 0.1). The Mrk IRAS galaxies do not follow the local TF relations for normal galaxies, as a significant proportion of them have a low value of $\log(V_m)$

The fact that the barred and unbarred galaxies show no difference in the TF plane is not specific to Mrk IRAS galaxies. We have verified that this is also true for the normal galaxies of Mathewson & Ford (1996). Courteau et al. (2003) reach a similar conclusion, but based on optical kinematics. This simply means that the presence of a bar does not affect the proportion of luminous to dark matter at a given radius.

We believe that the excess of galaxies with low V_m in Fig. 6 is real, and tells us something about the physical properties of Mrk IRAS galaxies. We next try to identify the origin of this effect, by investigating the 17 most deviant galaxies in the K -band TF diagram. They are indicated by a triangular symbol in both panels of Fig. 6; one can see that most of them are also deviant in the B -band TF relation. Their properties are listed in Table 4.

The HI distribution has been mapped in only two galaxies (Mrk 52 and 313) among those listed in Table 4. The HI distribution of Mrk 52 is well resolved, revealing a centrally peaked column density structure (Taylor et al. 1995). The velocity map of this galaxy indicates differential rotation, though it lacks spatial and velocity resolution to detect any asymmetries that might exist. High-resolution HI observations in the Mrk 313 group of galaxies reveal that the HI morphology of almost all the member galaxies are affected by the environment and four galaxies show tidally distorted HI morphology and kinematics (Li & Seaquist 1994). The HI emission of the pair NGC 7464/Mrk 313 is dominated by a ring around Mrk 313. The orientation of Mrk 313 and the ring suggest that it repre-

sents a polar ring around Mrk 313 and could be material pulled out of NGC 7464 during a close encounter with Mrk 313.

For the other galaxies, we have to rely on the HI profiles. Four of them are in Fig. 1, the others can be found in the literature. Only a few galaxies have a classical double-horned profile : Mrk 52, 307, 489, 592, and possibly Mrk 300 and 319. The others have a sloping profile, either gaussian or centrally peaked (Mrk 201, 331, 353, 691, 905, 1064, 1302) or a lopsided profile (Mrk 313, 471, 685, 1003, 1157). The gaussian/centrally peaked profiles suggest that the HI is centrally concentrated and does not extend to the flat part of the rotation curve, the lopsided profiles indicate uneven distribution of HI in the disk of the galaxy. In summary, such profiles indicate that the HI gas has not reached equilibrium in these galaxies.

Peculiar HI kinematics does not seem to be limited to active galaxies. We have examined the properties of the 7 galaxies which have an abnormally low $\log(V_m)$ in the K -band TF relation for the 682 normal galaxies (Mathewson & Ford 1996). Five of these galaxies (ESO 34-3, 446-2, 512-12, 563-13, 576-1) become “normal” again if one uses the maximum rotation velocity of the ionized gas instead of that of the HI gas. For the two other ones (ESO 384-32 and UGC 645) optical kinematics are not available. Thus peculiar HI kinematics in an otherwise normally rotating galaxy can also be found among normal galaxies, unless these objects are misclassified in terms of nuclear activity.

In order to better understand the cause of the slow rotation of the neutral HI gas in part of our sample, we have looked for correlations with other properties of the galaxies. Their en-

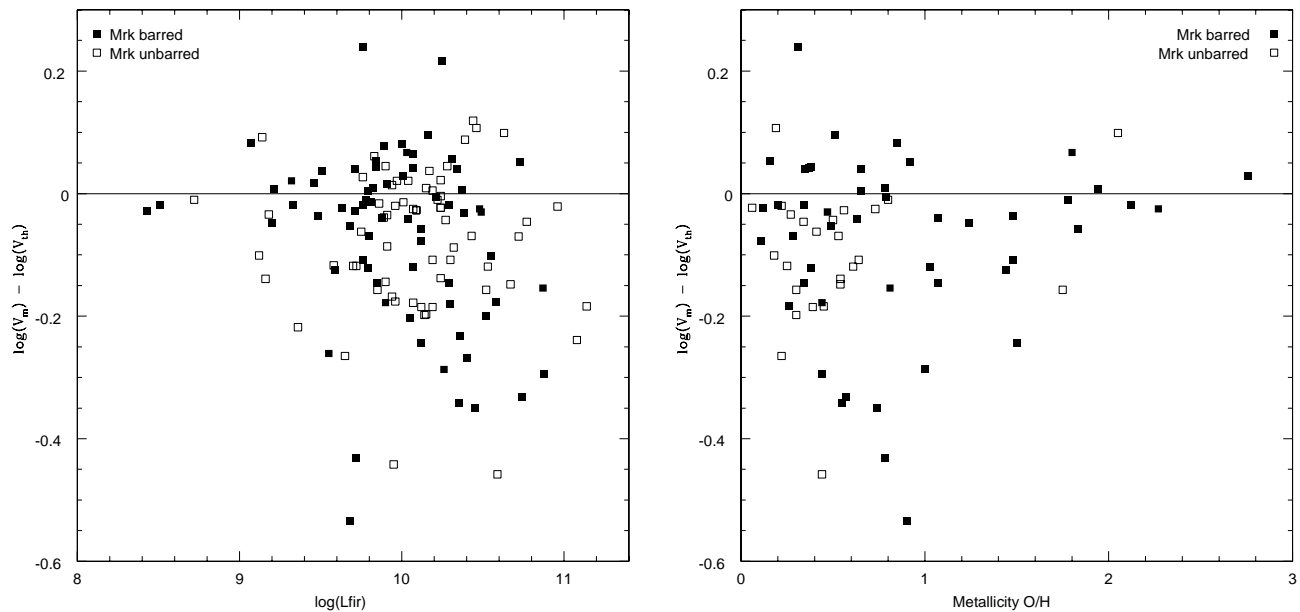


Fig. 7. Departure from the TF relation in the K band as a function of FIR luminosity (*left*), and oxygen abundance (O/H) (*right*). Like in Fig. 6, only data points with uncertainties in $\log(V_m)$ less than 0.1 and inclinations higher than 30° are plotted. The full and empty squares are the barred and unbarred galaxies respectively. The galaxies which depart most from the TF relation also have the strongest FIR luminosity and the lowest metallicity.

vironment, as determined from CCD and sky survey images, gives no indication to explain the perturbed kinematics : only one galaxy (Mrk 201) appears strongly disturbed, and another one (Mrk 313) is in a group, while the others are isolated or in rather distant pairs and fairly symmetric in shape (Table 4). The 17 deviant galaxies have on average a much higher HI mass excess ($\langle \Delta M_{HI} \rangle = 0.30$ and 0.33 for the barred and unbarred galaxies respectively, see Table 4) than the whole sample of Mrk IRAS galaxies (Table 2). As pointed out by the referee, applying the baryonic correction advocated by McGaugh et al. (2000) to these gas-rich galaxies makes them even more deviant, and thus even more peculiar.

The deviant galaxies also have a stronger FIR luminosity and a lower oxygen abundance. This is shown in Fig. 7, which give the difference between the observed V_m and that given by Eq. 8 as a function of FIR luminosity (L_{FIR} in L_\odot) and oxygen abundance (O/H) respectively. Only the data with an accuracy in $\log(V_m)$ better than 0.1 and an inclination larger than 30° are plotted. The same holds true for the departure from the TF relation in the B band. These trends are reinforced if one plots data with an accuracy in $\log(V_m)$ better than 0.2 (instead of 0.1). It thus appears that the most deviant galaxies are the youngest ones and those with the highest star formation rates, which is proportional to L_{FIR} .

6. Conclusions

The first objective of this paper was to search for differences in HI content between Mrk IRAS and “normal” galaxies, and between barred and unbarred galaxies. We compared the HI properties of two homogeneous samples of Mrk IRAS (mainly

starburst) and normal galaxies, with a further distinction between barred and unbarred objects. The main results of this comparative study can be summarized as follows.

Taking into account selection effects due to different distributions in distances and morphological type between normal and Mrk IRAS galaxies, we find that unbarred galaxies have more HI gas than barred ones. This is probably the most important result of this paper. Our interpretation is that the bar contributes efficiently to transforming the neutral hydrogen into molecular form, by funneling it into denser and dust-rich regions where most CO is detected : the leading edge of the bar (Sheth et al. 2002) and subsequently the central regions of the galaxy, where most star formation takes place. Note, however, that the bars of the Mrk IRAS galaxies are too young to have contributed to the actual central starburst (Coziol et al. 2000; Considère et al. 2000).

We also find that the Mrk IRAS galaxies have more neutral gas than normal galaxies. Although less robust, this result suggests that these galaxies have transformed less HI into stars because they are young, as testified by their metallicity (e.g. Coziol et al. 1997).

The other objective of this study was to investigate how the Mrk IRAS galaxies behave with respect to the TF relation, which is a fundamental scaling relation between the galaxy mass and its large-scale dynamics. We found that a significant fraction of Mrk IRAS galaxies strongly deviate from the TF relation defined for normal galaxies, both in the B and the K bands. This is the other striking result of this study and, as already pointed out by Coziol et al. (2000), an important property of starburst galaxies. However, the interpretation of these

deviations is not straightforward, because we have no detailed kinematic information on these galaxies.

Peculiar HI distribution and kinematics seem to be quite common among star-forming galaxies (e.g., Taramopoulos, Payne & Briggs 2001; Meurer, Staveley-Smith & Killeen 1998; Swaters, Sancisi & van der Hulst 1997; Hurt, Turner & Ho 1996; Kobulnicky & Skillman 1995). The motion of HI gas in the vertical direction has been studied in several nearby spiral galaxies. The general interpretation of these vertical motions is that they are the result of the formation and expansion of supershells around starburst nuclei due to stellar winds from massive OB stars and/or supernova explosions (e.g. Sancisi et al. 2001). Finally, Barton et al. (2001) have recently shown that a significant fraction of star-forming galaxies in close pairs deviate from the TF relation, with lower values of $\log(V_m)$. Although most of these outliers show signs of recent star formation, Barton et al. (2001) suggest that gas dynamical effects are probably the dominant cause of their anomalous TF properties, some of them showing signs of recent gas infall after a close galaxy-galaxy pass.

Most of the deviant galaxies in Table 4 are isolated, suggesting that strong gravitational interactions are not at the origin of the peculiar HI kinematics, except perhaps for Mrk 201 and 313. We assume that the HI gas has been recently accreted by these galaxies in minor merger events, and has not settled to dynamical equilibrium (lopsided profiles), or is partly in non-planar motion induced by superwinds (gaussian/centrally peaked profiles). A single minor merger is not sufficient to raise the HI mass excess by 0.15, since it would require that the typical merging dwarf contribute 40% of the HI mass of the galaxy. We thus have to assume either that our galaxies frequently suffered minor mergers (say 4 to 7 in their lifetime), which seems unprobable in view of their generally low metallicity (and thus age), or that they were initially gas-rich; a combination of the two possibilities is probably the correct scenario, since, as pointed out by the referee, gas-rich disks are likely to respond to mergers by more vigorous starburst.

How can we interpret these results in terms of the evolutionary stage of starburst galaxies?

In the framework of the hierarchical formation of galaxies, gravitational interactions play a fundamental role in galaxy evolution, primarily through minor galaxy-galaxy encounters. In the local universe, starburst nucleus galaxies are certainly the best examples of such processes. They frequently show signatures of recent interactions (e.g., Contini 1996) and have systematically lower metallicities than normal galaxies of similar masses and morphological types (Coziol et al. 1997), suggesting a particularly early evolutionary stage. Moreover, recent studies have shown that their bar structures were formed recently (age < 1 Gyr; Considère et al. 2000) mainly because these galaxies are still forming their disks (Coziol et al. 2000). A detailed and exhaustive study of their chemical abundances further revealed that the star formation history of starburst nucleus galaxies is probably dominated by a succession of starbursts extending over a few Gyr (Coziol 1996; Coziol et al. 1999; Mouhcine & Contini 2002). The most natural explanation for such a star formation scenario involves the trigger of

starbursts by gravitational interactions, mainly through minor mergers.

The results of this paper, which concerns both the global gas content and the large-scale HI dynamics in starburst galaxies, further support this evolutionary scenario. Starburst galaxies contain more neutral gas than normal ones because they recently underwent several minor mergers which increased their reservoir of HI gas and triggered nuclear starbursts. A significant fraction of these galaxies show strong deviations from the TF relations because the recently accreted HI gas has not had time to become stable in a regularly rotating disk and reach dynamical equilibrium. The fact that the most deviant galaxies are those with the highest star formation rates and the lowest metallicities is not surprising. The level of dynamical perturbations in the HI kinematics (measured by the departure from the TF relation), as well as the level of induced star formation (measured by L_{FIR}) should scale in principle with the intensity of the latest gravitational interaction undergone by the galaxy. Following the well-known scaling relation between metallicity and mass, metal-poor galaxies have small masses and are thus more affected by interactions than massive ones, explaining the observed trend in Fig. 7.

As predicted by numerical simulations, low-level gravitational interactions are the best way to initiate instabilities in the stellar galactic disk and thus to form a bar. This could explain why bars are so “young” in starburst galaxies: their disks are still forming and they suffered recent minor interactions. The difference in HI content between barred and unbarred galaxies – the latter being richer – could be explained by the efficiency of bars in driving gas toward denser and dust-richer regions of galaxies, where it is transformed into molecular clouds on its way to forming stars. Following this scenario, barred galaxies should contain more molecular gas than unbarred ones. We are investigating this prediction thanks to new CO observations of Mrk starburst galaxies (Contini et al., in preparation).

Over the past few years, considerable progress has been achieved in our understanding of galaxy formation and evolution. In particular, deep photometric and spectroscopic surveys performed on the largest telescopes reveal populations of luminous star-forming galaxies up to redshifts 3 – 4. Even if it remains unclear whether these objects are representative of the whole galaxy population that exists in the distant universe, the starburst phenomenon appears now as a key process in galaxy evolution.

Acknowledgements. We thank the technical staff of Observatoire de Nançay for their help in acquiring the data, and Gilles Theureau for help with the absolute calibration. We acknowledge with thanks detailed constructive comments from an anonymous referee, which considerably improved the paper. This research has made use of LEDA (the Lyon-Meudon Extragalactic Database; <http://leda.univ-lyon1.fr>), and of NED (the NASA/IPAC Extragalactic Database; <http://nedwww.ipac.caltech.edu>) which is operated by the Jet Propulsion Laboratory, California Institute of Technology, under contract with the National Aeronautics and Space Administration.

References

- Andreani P., Casoli F., Gerin M., 1995, *A&A*, 300, 43
- Balzano V.A., 1983, *ApJ*, 268, 602
- Barton E. J., Geller M. J., Bromley B. C., van Zee L., Kenyon S. J., 2001, *AJ*, 121, 625
- Boselli A., 1994, *A&A*, 292, 1
- Burstein D., Sarazin C. L., 1983, *ApJ*, 264, 427
- Bushouse, H. A., 1987, *ApJ* 320, 49
- Chapelon S., Contini T., Davoust E., 1999, *A&A*, 345, 81 (paper V)
- Cole S., Aragon-Salamanca A., Frenk C. S., Navarro J. F., Zepf S. E., 1994, *MNRAS*, 271, 781
- Considère S., Coziol R., Contini T., Davoust E., 2000, *A&A*, 356, 89 (paper IV)
- Contini T., 1996, Ph. D. thesis, Université Pau. Sabatier, Toulouse, France
- Contini T., Considère S., Davoust E., 1998, *A&AS*, 130, 285 (paper III)
- Contini T., Davoust E., Considère S., 1995, *A&A*, 303, 440 (paper I)
- Contini T., Wozniak H., Considère S., Davoust E., 1997a, *A&A*, 324, 41 (paper II)
- Contini T., Wozniak H., Considère S., Davoust E., 1997b, *A&A*, 318, L51
- Courteau S., 1997, *AJ*, 114, 2402
- Courteau S., Andersen D.R., Bershadsky M.A., MacArthur L.A., Rix H.-W., 2003, *ApJ*, 594, 208
- Courteau S., Rix H., 1999, *ApJ*, 513, 561
- Coziol R., 1996, *A&A*, 309, 345
- Coziol R., Torres C.A.O., Quast G.R., Contini T., Davoust E., 1998, *ApJS*, 119, 239
- Coziol R., Contini T., Davoust E., Considère S., 1997, *ApJ*, 481, L67
- Coziol R., Considère S., Davoust E., Contini T., 2000, *A&A*, 356, 102
- Dahari O., De Robertis M.M., 1988, *ApJS* 67, 249
- Davis, L. E., Seaquist E. R., 1983, *ApJS* 53, 269
- Deharveng J-M., Sasseen T. P., Buat V., Bowyer S., Lampton M., Wu X., 1994, *A&A*, 289, 715
- de Vaucouleurs, G. de Vaucouleurs, A., Corwin, H.G., et al., 1991, *Third Reference Catalogue of Bright Galaxies* Springer Verlag.
- Donas J., Milliard B., Laget M., Buat V., 1990, *A&A*, 235, 60
- Eisenstein D. J., Loeb A., 1996, *ApJ*, 459, 432
- Eskridge P. B., Pogge R. W., 1991, *AJ*, 101, 2056
- Faber S. M., Jackson R. E., 1976, *ApJ*, 204, 668
- Fouqué P., Bottinelli L., Durand N., et al. 1990, *A&AS* 86, 473
- Friedli D., Benz W., 1993, *A&A*, 268, 65
- Friedli D., Benz W., 1995, *A&A*, 301, 649
- Garcia, A. M.; Bottinelli, L.; Garnier, R, et al. 1994, *A&AS* 107, 265
- Giovanelli, R., Haynes, M. P., 1985, *AJ* 90, 2445
- Giovanelli R., Haynes M.P., 1988, in “Galactic and Extragalactic Radio Astronomy”, G. L. Verschuur & K. I. Kellermann (eds.), Springer-Verlag, p. 522
- Giovanelli, R., Haynes, M. P., 1993, *AJ* 105, 1271
- Haynes M.P., Giovanelli R., 1984, *AJ*, 89, 758
- Haynes, M. P., Giovanelli, R., 1991, *ApJS* 77, 331
- Haynes, M. P., Giovanelli, R., Herter, T., 1997, *AJ* 113, 1197
- Heckman, T. M.; Balick, B.; Sullivan, W. T. III, 1978, *ApJ* 224, 745
- Henning, P. A., 1992, *ApJS* 78, 365
- Hunter D. A., Hunsberger S. D., Roye E. W., 2000, *ApJ*, 542, 137
- Hurt R. L., Turner J. L., Ho P. T. P., 1996, *ApJ*, 466, 135
- Jackson J. M., Barrett A. H., Armstrong J. T., Ho P. T. P., 1987, *AJ*, 93, 531
- Keel W. C., van Soest E. T. M., 1992, *A&AS*, 94, 553
- Kennicutt R. C., 1989, *ApJ*, 344, 685
- Kennicutt R. C., 1998, *ApJ*, 498, 541
- Kobulnicky H. A., Skillman E. D., 1995, *ApJ*, 454, L121
- Koda J., Sofue Y., Wada K., 2000, *ApJ*, 532, 214
- Li J. G., Seaquist E. R., 1994, *AJ*, 107, 1953
- Martin J.-M., Bottinelli L., Dennefeld M., Gougenheim L., 1991, *A&A* 245, 393
- Mathewson D.S., Ford V.L., 1996, *ApJS* 107, 97
- Matthews L. D., van Driel W., Gallagher J. S., 1998, *AJ* 116, 2196
- Mazzarella J.M., Balzano V.A., 1986, *ApJS* 62, 751
- Mazzarella J.M., Boroson T.A., 1993, *ApJS* 85, 27
- McGaugh S. S., Schombert J. M., Bothun G. D., de Blok W. J. G., 2000, *ApJ*, 533, L99
- Meurer G. R., Staveley-Smith L., Killeen N. E. B., 1998, *MNRAS*, 300, 705
- Mihos J. C., Hernquist L., 1994, *ApJ*, 425, L13
- Mirabel I. F., Sanders D. B., 1988, *ApJ*, 335, 104
- Mo H. J., Mao S., 2000, *MNRAS*, 318, 163
- Mouhcine M., Contini T., 2002, *A&A* 389, 106
- Mouhcine M., Lançon., 2003, *A&A* 402, 425
- Navarro J. F., Steinmetz M., 2000, *ApJ*, 538, 477
- Noguchi, M. 1988, *A&A*, 203, 259
- O’Neil K., Bothun G. D., Schombert J., 2000, *AJ*, 119, 136
- Paturol G., Fouqué P., Buta R., Garcia A.M., 1991, *A&A* 243, 319
- Pierce M. J., Tully R. B., 1992, *ApJ*, 387, 47
- Sheth, K., Vogel, S.N., Regan, M.W. et al., 2002, *AJ* 124, 2581
- Rubin V. C., Burstein D., Ford W. K., Thonnard N., 1985, *ApJ*, 289, 81
- Sancisi R., Fraternali F., Oosterloo T., van Moorsel G., 2001, in “Galaxy disks & disk galaxies”, ASP Conf. Series, J.G. Funes & E.M. Corsini (eds.), p.111
- Shlosman I., Frank J., Begelman M. C., 1989, *Nature*, 338, 45
- Smoker, J. V.; Davies, R. D.; Axon, D. J.; Hummel, E., 2000, *A&A* 361, 19
- Steinmetz M., Navarro J. F., 1999, *ApJ*, 513, 555
- Swaters R. A., Sancisi R., van der Hulst J. M., 1997, *ApJ*, 491, 140
- Taramopoulos A., Payne H., Briggs F. H., 2001, *A&A*, 365, 360
- Taylor C. L., Brinks E., Grashuis R. M., Skillman E. D., 1995, *ApJS*, 99, 427
- Theureau G., Bottinelli L., Coudreau-Durand N., et al. 1998, *A&AS* 130, 333
- Thuan T.X., Lipovetsky V.A., Martin J.-M. et al., 1999, *A&AS* 139, 1
- Tully R.B., Fisher J.R., 1977, *A&A* 54, 661
- Tully R. B., Pierce M. J., 2000, *ApJ*, 533, 744
- van den Bosch F. C., 2000, *ApJ*, 530, 177
- Zaritsky D., Rix H., 1997, *ApJ*, 477, 118

Table 5. HI data for Markarian galaxies observed at the Nançay Radiotelescope. The Mrk number is in col. 1, the radial heliocentric HI velocity and its error (in km s^{-1}) in cols. 2 and 3, the rms noise in the profile (in Jy) in col. 4, the signal-to-noise ratio (SNR) in col. 5, the measured linewidths at 20 and 50% of maximum intensity (in km s^{-1}) in cols. 6 and 7. When no line was detected, the listed $W50$ was estimated from the Tully-Fisher relation. The HI flux F_{HI} (or an upper limit) and its uncertainty (in Jy km s^{-1}) are given in cols. 8 and 9. The last galaxy of that Table is UGCA 304, the companion of Mrk 1337.

Mrk	t	incl	V_{\odot}	ΔV_{\odot}	rms	SNR	$W20$	$W50$	F_{HI}	ΔF_{HI}
(1)	(2)	[deg]	[km s^{-1}]	[km s^{-1}]	[mJy]	(7)	[km s^{-1}]	[km s^{-1}]	[Jy km s^{-1}]	[Jy km s^{-1}]
(1)	(2)	(3)	(4)	(5)	(6)	(7)	(8)	(9)	(10)	(11)
21	3.6	58	8433	18	7.1	3.4	301	236	1.37	0.80
38	3.4	70	10813	28	6.7	3.2	287	148	1.70	0.82
42	2.7	38	[7200]		10.1			[132]	<3.98	
54	5.1	69	13450	16	4.8	3.2	225	185	1.64	0.68
78		50	[11194]		9.1			[236]	<6.45	
84	3.6	62	6098	19	5.7	5.0	310	158	4.30	0.99
90	3.8	29	4253	13	4.5	4.0	264	221	2.74	0.78
103	4.8	29	[9353]		8.8			[167]	<4.40	
109	8.0	50	9054	7	5.6	8.0	308	251	7.47	1.01
122	2.0	63	[6538]		10.1			[289]	<8.78	
141	-4.9		[12265]		12.1			[141]	<5.11	
144	4.8	25	[8253]		9.6			[118]	<3.39	
152	2.7	68	[6896]		7.6			[277]	<6.28	
236	2.7	47	14895	19	10.4	4.4	259	142	3.77	1.32
237	3.4	38	8937	13	3.9	3.3	186	160	2.13	0.70
238	4.9	27	14884	31	6.3	3.3	283	110	1.90	0.84
262		71	8918	25	8.1	2.8	208	129	2.44	1.11
264			[18746]		10.6			[154]	<4.87	
271	3.1	42	7541		6.2	3.4	340	243	2.41	0.74
288	4.9	74	[7500]		9.2			[227]	<6.25	
291	1.1	47	[10552]		6.1			[198]	<3.61	
306	4.0	57	5609	8	5.4	8.9	257	176	7.89	0.96
311	4.8	19	9190	15	4.4	3.7	310	261	1.37	0.55
333	-1.8	37	4811	7	5.1	2.6	117	111	1.15	0.66
359	2.7	38	[5043]		4.5			[162]	<2.19	
373		53	5903	26	5.1	3.1	229	121	1.91	0.78
374	2.7	69	12780	8	15.5	6.9	121	74	8.54	1.94
382	4.6	25	10099	16	5.1	3.2	189	149	1.15	0.59
412	7.5	71	4479	6	4.9	7.4	166	127	4.09	0.73
414	1.7	57	11350	7	4.0	4.7	461	443	2.36	0.62
445	4.2	61	[4600]		6.4			[182]	<3.49	
455	9.7	61	10175	37	4.7	2.9	375	180	1.75	0.74
474		38	[10732]		2.6			[222]	<1.71	
551	3.6	44	[15061]		17.8			[228]	<12.20	
552	-0.3	32	4349	8	17.2	7.3	299	237	23.81	3.32
558	-1.3	43	[3957]		14.4			[160]	<6.92	
592	3.1	52	7716	5	9.0	5.1	181	167	5.73	1.39
596	4.2	32	11594	20	12.9	5.6	432	222	12.19	2.35
607	1.1	81	2663	16	3.8	4.4	133	51	0.74	0.35
618	3.0	44	10684	20	4.0	4.3	308	192	2.84	0.71
623	3.8	49	12617	10	3.6	5.7	128	74	1.04	0.37
626	0.3	5	3933	7	5.7	4.7	66	47	1.02	0.49
661	4.8	58	[10606]		11.1			[261]	<8.70	
665	5.5	57	7630	17	6.7	3.3	228	174	2.18	0.92
688	2.0	49	11539	10	4.2	6.7	260	190	4.63	0.74
712	3.6	63	4565	12	7.7	7.4	323	202	9.25	1.38
718	5.4	26	8517	14	4.6	4.3	241	182	2.09	0.67
721	4.9	38	9621	16	3.2	5.7	243	96	1.26	0.37
731	-1.3	49	1453	10	3.9	4.1	212	183	2.32	0.63
766	1.0	39	[3819]		4.6			[94]	<1.28	
785	1.3	42	14750	23	4.8	2.9	307	235	1.42	0.68
804	4.9	33	5365	16	3.7	4.3	253	179	1.89	0.58
827	4.1	74	5464	8	7.3	7.7	346	282	11.64	1.47
834	2.0	27	10802	20	6.4	5.2	377	204	3.88	0.96
851	1.7	18	10665	13	3.8	4.1	197	153	0.90	0.39
860	3.4	62	6868	10	4.1	4.6	140	104	1.50	0.52
861	4.9	21	4398	14	4.7	5.0	217	146	2.64	0.69
874	3.4	48	4080	7	4.7	7.2	168	127	4.01	0.72
881	5.5	49	8682	13	6.4	4.7	226	164	3.40	0.96
898	3.1	54	5072	13	4.2	4.0	296	256	1.94	0.63
899	3.8	27	5525	13	8.2	4.8	170	108	4.28	1.19
905	-1.8	53	4703	5	12.9	7.8	135	110	9.87	1.78
910	1.1	38	4910	16	5.6	3.5	282	232	1.95	0.78
912	0.1	63	[4845]		15.6			[238]	<11.13	
922	4.9		6574	10	8.2	5.4	145	95	3.18	0.99
928	-0.9	40	7250	13	4.7	5.9	145	57	1.73	0.51
929	3.4	49	5259	16	5.3	4.3	296	223	4.43	1.04
936	3.1	73	[9059]		14.8			[343]	<15.21	
937	5.3	28	8846	16	5.6	5.7	205	68	2.39	0.68
943	3.9	61	5186	19	3.9	4.5	245	128	1.80	0.56

Table 6. HI data for Markarian galaxies observed at the Nançay Radiotelescope (*continued*)

Mrk	t	incl	V_{\odot}	ΔV_{\odot}	rms	SNR	W_{20}	W_{50}	F_{HI}	ΔF_{HI}
(1)	(2)	[deg]	[km s^{-1}]	[km s^{-1}]	[mJy]	(7)	[km s^{-1}]	[km s^{-1}]	[Jy km s^{-1}]	[Jy km s^{-1}]
955	4.2	61	10490	26	6.2	3.0	246	149	1.47	0.78
966	0.4	47	5335	16	5.5	2.3	156	133	0.75	0.60
968	4.0	24	4553	5	10.7	8.0	170	137	11.01	1.67
997	4.2	63	5795	5	6.3	11.7	320	243	14.53	1.23
1026	2.0	45	3994	8	8.3	8.2	271	205	12.87	1.59
1039	5.0	75	2111	5	6.7	8.3	161	134	6.16	0.97
1043	0.2	48	2435	13	4.0	4.0	172	133	1.86	0.60
1058	4.8	66	[5138]		4.8			[215]	<3.07	
1064	-1.9	39	4644	5	6.9	12.7	173	101	9.34	1.00
1066	-1.2	68	3605	30	3.9	3.5	280	104	1.11	0.53
1076	4.0	67	[7232]		4.1			[229]	<2.84	
1081	1.7	20	5327	10	5.0	6.4	284	222	5.76	0.94
1085	4.2	59	5127	16	5.6	6.0	354	217	5.22	0.97
1086	2.7	42	9043	13	5.2	5.6	287	208	4.30	0.89
1092	3.1	76	3356	3	5.9	14.7	338	311	19.90	1.22
1104	2.1	27	1991	37	11.0	1.4	155	109	16.85	4.99
1116	4.9	37	7823	16	11.9	3.0	283	246	2.68	1.43
1149	5.0	63	6292	5	4.4	5.8	276	262	4.29	0.79
1180		46	[4534]		6.0			[213]	<3.82	
1197	4.2	57	4958	18	3.4	3.5	298	235	2.11	0.64
1198	3.5	69	7635	10	8.4	4.9	509	466	9.63	1.79
1199	2.7	43	4085	17	6.2	4.9	171	60	1.78	0.67
1200	2.7	26	7788	8	4.3	6.2	293	253	4.45	0.77
1270	5.0	44	8307	14	7.9	5.8	299	196	7.60	1.41
1273		55	8184	50	6.1	2.2	382	179	1.29	0.71
1302	3.0	62	5588	2	5.5	14.8	108	92	7.00	0.71
1337	2.1	54	2556	5	5.8	8.0	251	231	7.91	1.05
1344	-2.0	31	3170	7	7.2	9.5	182	101	6.44	0.97
1356	1.7	45	11872	25	6.4	2.8	157	83	0.80	0.60
1361		25	[6768]		6.2			[185]	<3.44	
1363	1.1	34	2743	3	6.8	9.9	206	197	9.46	1.09
1403	4.8	53	8693	11	5.4	5.1	191	144	2.54	0.73
1404	4.8	27	[10687]		9.4			[168]	<4.75	
1425	4.5	61	7480	7	5.0	5.1	280	258	5.25	1.00
1452	4.9	41	6680	12	5.6	5.5	200	131	4.18	0.92
UA 304		90	2176	8	5.7	12.7	245	66	3.94	0.59

Table 7. Integrated quantities for the Mrk IRAS galaxies. The Mrk number is in col. 1, the morphological type (SA = unbarred, SB = barred) in col. 2, the spectral type (stb = starburst; sy = Seyfert; st? and sy? are classifications from an IRAS color index as explained in text) in col. 3, the numerical morphological type t (RC3) in col. 4, the inclination (in degrees) in col. 5, the isophotal diameter d_c and its uncertainty (in log of 0.1') in cols. 6 and 7, the maximum rotation velocity V_m and its uncertainty in log(km s⁻¹) in cols. 8 and 9, the distance D (in Mpc) in col. 10, the K -band magnitude in col. 11, the oxygen abundance (O/H) with respect to solar in col. 12, the total HI mass and its uncertainty (in M_\odot) in cols. 13 and 14, the total FIR luminosity (in L_\odot) in col. 15 and the absolute blue magnitude M_B in col. 16.

Mrk	Bar	Spe	t	incl.	log(d_c)		log(V_m)		D	m_K	O/H	log(M_{HI})		log(L_{FIR})	M_B
(1)	(2)	(3)	(4)	(5)	(6)	(7)	(8)	(9)	(10)	(11)	(12)	(13)	(14)	(15)	(16)
				[deg]	[0.1']		[km s ⁻¹]		[Mpc]	[mag]	[\odot]	[M_\odot]		[L_\odot]	[mag]
1	SB	sy2	3.1	56.8	0.871	0.051	2.122	0.029	65.9	11.17	0.11	9.57	0.24	10.12	-19.73
2	SB	stb	0.6	27.2	0.850	0.051	2.251	0.232	75.7	10.64	1.61	9.47	0.30	10.64	-20.75
4	SB	stb	6.0	63.2	1.283	0.042	2.111	0.045	73.9	10.41		9.58	0.30	10.30	-20.81
8	SA	stb	4.1	62.7	0.943	0.044	2.067	0.044	51.3	11.88	0.22	9.73	0.27	9.96	-19.94
10	SB	sy1	3.1	68.4	1.229	0.050	2.430	0.018	119.6	10.35	0.65	10.63	0.10	10.34	-22.69
12	SA	stb	5.0	38.0	1.056	0.052	2.245	0.088	56.1	10.21	0.80	10.08	0.10	10.22	-21.10
13	SB	stb	3.1	31.5	1.023	0.084	2.544	0.162	21.9	11.80	0.61	9.55	0.10	8.59	-17.76
21	SB	stb	3.6	58.2	0.983	0.054	2.196	0.096	115.4	11.11	1.03	9.63	0.58	10.07	-21.04
31	SB	stb	2.5	35.9	0.936	0.066	2.146	0.136	107.1	11.25	1.70	9.76	0.10	10.01	-20.23
38	SB	stb	3.4	70.2	0.856	0.056	2.058	0.204	147.2	12.25	0.59	9.94	0.48		-20.93
52	SB	stb	-0.7	63.5	1.327	0.046	1.734	0.058	29.0	9.78	0.78	9.00	0.24	9.72	-19.37
54	SA	stb	5.1	68.9	0.881	0.063	2.029	0.125	181.3	12.84	0.25	10.10	0.41	10.68	-21.83
58	SB	stb	1.3	31.0	0.761	0.048	2.471	0.112	74.0	12.28	0.97	8.69	0.30	9.48	-19.36
79	SB	sy2	3.0	28.2	1.142	0.052	2.256	0.208	91.0	9.80		9.90	0.08	10.24	-21.48
84	SA	st?	3.6	62.2	1.001	0.073	2.119	0.120	84.1	11.14		9.86	0.23	10.18	-21.25
86	SB	stb	8.4	35.0	1.512	0.293	1.874	0.280	6.9	9.46	0.36	8.65	0.12	8.66	-17.36
87	SB	stb	1.0	47.5	1.118	0.084	2.154	0.049	51.1	9.78	0.38	9.87	0.30	9.79	-20.12
90	SB	stb	3.8	29.4	0.889	0.075	2.390	0.044	59.3	10.64		9.36	0.28	9.74	-20.32
101	SA	stb	4.6	17.6	0.880	0.097	2.174	0.545	66.0	10.94	0.51	9.69	0.30	9.87	-20.42
109	SB	stb	8.0	49.7	0.529	0.041	2.256	0.032	123.7	12.97	0.51	10.43	0.14	10.16	-19.36
114	SB	stb	3.1	28.7	1.182	0.046	2.326	0.167	103.4	10.80	0.43	10.30	0.10	10.42	-20.61
133	SB	stb	4.0	12.3	1.054	0.045	2.499	1.256	31.2	9.94	1.74	9.22	0.12	9.66	-19.30
158	SA	stb	1.0	67.7	1.232	0.045	2.021	0.018	31.7	9.59		9.02	0.08	10.07	-19.77
161	SB	stb	4.1	52.6	0.883	0.071	1.861	0.103	82.5	10.75	0.74	9.99	0.30	10.39	-21.14
179	SB	stb	5.3	35.9	1.163	0.072	2.110	0.081	47.7	10.09	1.44	9.36	0.14	9.59	-19.98
185	SB	stb	5.9	42.6	1.353	0.042	2.270	0.061	44.2	9.70		9.95	0.13	9.91	-20.80
188	SB	stb	5.3	39.7	1.264	0.056	2.280	0.095	35.3	9.25	2.76	9.70	0.10	10.01	-20.43
201	SA	stb	9.8	60.1	1.261	0.071	1.766	0.093	36.7	9.63	0.44	9.33	0.30	10.59	-20.48
207	SA	st?	1.0	42.6	1.116	0.053	1.908	0.158	36.8	10.38		9.19	0.27	9.67	-19.70
213	SB	stb	1.1	49.2	1.210	0.052	2.294	0.059	45.0	9.75	0.37	9.40	0.33	10.07	-20.55
236	SA	sy1	2.7	47.0	0.819	0.055	2.130	0.117	210.0	11.84		10.58	0.35	10.20	-21.10
237	SA	stb	3.4	38.4	0.732	0.082	2.129	0.080	123.8	12.01	0.61	9.89	0.33	10.53	-19.84
238	SA	stb	4.9	26.6	0.933	0.046	2.315	0.125	201.7	11.52	0.84	10.26	0.44	10.92	-21.79
256	SA	st?	5.0	42.1	1.050	0.066	2.164	0.080	45.6	11.01		9.64	0.18	9.97	-20.07
262	SB	stb		71.3	0.620	0.050	1.937	0.241	123.8	13.15	0.41	9.95	0.45		-18.88
271	SB	stb	3.1	41.5	0.906	0.048	2.339	0.088	104.3	10.29	0.47	9.79	0.31	10.49	-21.21
281	SB	stb	3.1	40.0	1.422	0.057	2.366	0.081	32.9	8.72		9.75	0.35	10.00	-20.64
286	SA	stb	4.2	30.3	0.951	0.044	2.355	0.156	105.1	10.58	0.44	10.29	0.10	10.84	-21.39
297	SA	stb	5.0	41.9	0.932	0.059	2.481	0.084	65.2		0.56	9.93	0.29	10.62	-21.34
300	SB	stb	-0.1	59.5	0.847	0.102	2.006	0.042	159.9	11.36	0.74	9.86	0.30	10.45	-21.27
306	SB	stb	4.0	56.6	1.045	0.043	2.106	0.052	76.2	12.06	0.63	10.03	0.12	10.04	-20.24
307	SB	stb	4.6	35.0	1.068	0.047	2.004	0.088	75.6	10.46	1.00	9.82	0.18	10.26	-21.19
308	SA	stb	0.0	52.7	0.858	0.090	2.345	0.047	96.5	11.58	0.19	9.94	0.28	10.46	-20.39
311	SB	st?	4.8	19.0	0.641	0.114	2.636	0.029	123.5	11.25		9.69	0.40	10.65	-20.91
313	SB	sy2	-1.9	61.9	1.092	0.074	1.914	0.073	27.3	9.54		9.55	0.38	9.55	-19.18
318	SA	sy?	3.8	37.1	0.910	0.038	2.218	0.097	60.0	10.92		9.74	0.25	9.94	-20.14
319	SB	stb	1.1	53.4	1.099	0.076	2.053	0.057	109.3	10.63	0.44	9.98	0.22	10.88	-21.67
321	SA	sy?	5.9	15.3	1.046	0.063	2.632	0.467	129.3	10.32		10.51	0.21	10.88	-22.27
323	SB	stb	5.9	47.0	1.097	0.079	2.275	0.042	58.6	9.88		9.48	0.20	10.29	-21.01
325	SA	st?	4.9	43.4	1.142	0.096	1.972	0.209	46.8	10.73	0.38	9.65	0.23	10.19	-20.33
326	SB	stb	4.0	55.7	1.191	0.075	2.166	0.044	48.8	10.26	1.83	9.76	0.24	10.12	-20.04
331	SA	st?	1.0	48.6	0.957	0.063	2.099	0.050	73.7	9.88		9.98	0.21	11.08	-20.21
332	SB	stb	4.2	24.3	1.165	0.050	1.935	0.223	33.2	9.37	0.81	9.05	0.13	9.94	-20.14
339	SB	stb		21.5	0.962	0.085	2.286	0.039	71.0	11.74		9.73	0.30	9.68	-20.13
353	SB	stb	2.2	65.0	0.950	0.046	1.927	0.030	63.2	10.31	0.55	9.32	0.28	10.35	-19.88
358	SB	sy1	4.0	42.2	0.896	0.081	2.396	0.051	182.1	11.27		10.16	0.24	10.37	-21.51
359	SB	sy1	2.7	38.0	0.889	0.068	1.933	0.114	68.3	10.46	0.30	8.85	0.30	9.91	-20.43
363	SA	stb	-2.0	36.5	0.793	0.115	2.063	0.074	40.1	10.93	0.41	9.39	0.32	9.75	-19.23
373	SB	stb		53.1	0.890	0.050	2.026	0.204	81.3	11.29	0.64	9.47	0.41	10.23	-19.77
374	SB	sy1	2.7	69.1	0.824	0.127	1.673	0.142	176.8	11.11		10.80	0.23		-22.38
382	SB	sy1	4.6	25.3	0.836	0.078	2.285	0.069	137.0	11.47		9.71	0.51	9.91	-20.42
384	SB	stb	3.0	54.8	1.151	0.042	2.283	0.032	63.4	9.82		9.29	0.19	10.38	-20.82
386	SB	stb	3.8	67.2	1.275	0.047	2.337	0.027	48.5	9.39		9.90	0.19	9.51	-20.84
389	SA	st?	1.0	29.2	1.276	0.070	2.408	0.158	64.1	9.31		10.01	0.16	9.78	-21.12
391	SA	stb	1.1	53.3	1.091	0.065	2.230	0.060	55.0	10.27		9.39	0.25	9.86	-20.25
401	SB	stb	0.5	34.9	1.031	0.045	1.978	0.156	24.1	10.31	1.47	8.83	0.27	9.32	-18.15
412	SB	stb	7.5	70.5	0.764	0.074	1.869	0.068	61.7	12.67	0.26	9.56	0.18	9.52	-19.22
414	SA	sy?	1.7	57.1	0.805	0.060	2.424	0.022	153.9	11.50		10.12	0.26	10.39	-21.30
430	SA	stb	0.0	59.4	1.310	0.054	2.195	0.027	81.1	9.81		9.96	0.10	9.94	-21.73
432	SA	stb	9.9	90.0	1.223	0.096	2.146	0.030	47.0	10.74	0.56	10.30	0.15	10.09	-20.26
446	SB	stb	3.1	40.8	1.148	0.083	1.948	0.132	97.0	10.35	0.80	9.92	0.17	10.31	-21.40

Table 8. Integrated quantities for the Mrk IRAS galaxies (*continued*)

Mrk	Bar	Spe	t	incl.	$\log(d_c)$		$\log(V_{\text{in}})$		D	m_K	O/H	$\log(M_{\text{HI}})$		$\log(L_{\text{FIR}})$	M_B
(1)	(2)	(3)	(4)	[deg]	[0.1']	[0.1']	[km s ⁻¹]	[km s ⁻¹]	[Mpc]	[mag]	[\odot]	[M_{\odot}]	[M_{\odot}]	[M_{\odot}]	[mag]
455	SA	st?	9.7	61.4	0.733	0.138	2.201	0.194	138.9	12.36		9.90	0.42	10.66	-20.70
471	SB	sy2	1.2	53.1	0.946	0.056	2.124	0.061	139.6	10.66		9.79	0.19	10.40	-21.69
479	SA	stb	3.9	60.8	1.013	0.062	2.219	0.039	83.0	10.98	0.50	10.05	0.19	10.27	-21.17
489	SB	stb	2.3	51.3	0.915	0.092	1.991	0.058	130.9	11.30	0.57	10.58	0.10	10.74	-21.55
493	SB	sy1	3.1	42.1	1.000	0.073	1.220	0.166	128.9	10.98		9.81	0.21	10.23	-20.93
496	SA	stb	1.7	68.7	0.796	0.223	2.150	0.022	121.8	11.02	0.45	10.07	0.30	11.14	-21.66
527	SB	stb	1.1	56.9	1.153	0.083	1.541	0.105	47.6	10.07		9.22	0.12	10.17	-19.90
529	SA	stb	-1.0	90.0	1.129	0.051	2.024	0.035	47.1	11.09	0.25	10.18	0.26	9.72	-18.95
531	SA	st?	-1.8	58.3	1.211	0.060	2.163	0.031	48.0	9.70		8.37	0.30	10.19	-20.03
533	SB	sy2	3.9	24.1	0.997	0.141	2.621	0.202	117.3	9.79		10.35	0.20	11.03	-21.92
534	SA	stb	-1.3	59.2	1.180	0.145	2.164	0.081	68.7	10.02	0.54	9.84	0.45	10.67	-21.11
538	SB	stb	3.1	50.0	1.299	0.085	2.070	0.086	37.3	9.76	0.34	9.80	0.17	10.29	-20.42
545	SB	stb	1.2	42.4	1.279	0.080	2.446	0.079	62.2	8.88	0.92	9.89	0.18	10.73	-21.47
552	SB	st?	-0.3	32.4	0.618	0.147	2.399	0.027	58.0	11.09		10.28	0.14	10.25	-19.87
554	SA	sy?	-2.0	41.6	1.169	0.098	2.105	0.074	70.4	11.06		9.73	0.30	9.70	-20.09
555	SA	stb	3.2	29.2	1.106	0.057	2.141	0.237	53.7	9.66		9.66	0.30	10.29	-21.22
565	SA	sy?	-2.0	43.2	1.316	0.053	2.352	0.079	72.5	9.75		9.22	0.30	10.19	-21.54
571	SB	stb	3.4	50.4	1.216	0.081	2.342	0.047	68.1	10.41	1.80	9.80	0.30	10.03	-20.48
572	SA	st?	7.9	83.0	1.079	0.057	2.299	0.034	65.4	10.47		9.09	0.34	10.17	-20.21
575	SB	stb	1.0	32.4	0.991	0.051	2.077	0.121	73.3	10.25	0.82	9.69	0.21	10.39	-20.48
592	SB	stb	3.1	52.0	0.994	0.142	2.022	0.040	102.3	11.52		10.15	0.24	10.36	-20.47
593	SB	stb	5.3	24.6	1.113	0.042	2.363	0.230	110.1	10.15		10.22	0.17	10.30	-21.50
596	SA	sy2	4.2	31.8	0.932	0.115	2.495	0.053	142.6	10.89		10.74	0.19	10.44	-21.70
602	SB	stb	4.0	34.0	1.102	0.080	2.294	0.157	37.2	10.11	1.34	9.70	0.24	9.86	-19.52
607	SA	sy2	1.1	80.9	1.275	0.076	1.582	0.349	34.8	9.36		8.33	0.47	9.57	-19.80
617	SB	stb	4.9	35.0	1.174	0.073			62.0	9.55	0.69	9.53	0.30	11.20	-21.34
618	SB	sy1	3.0	43.9	0.964	0.076	2.255	0.093	137.8	10.45	0.81	10.10	0.25	10.87	-22.44
620	SB	sy2	1.0	52.4	1.488	0.074	2.323	0.057	27.3	8.48	0.16	9.30	0.07	9.84	-20.16
623	SA	sy?	3.8	49.2	0.924	0.051	1.781	0.138	169.4	12.53		9.85	0.36	10.63	-21.24
626	SA	sy?	0.3	5.0	0.826	0.062	2.390	0.024	53.8	10.65		8.84	0.48	9.67	-19.64
665	SB	stb	5.5	57.2	0.998	0.118	2.069	0.121	108.3	11.26	0.41	9.78	0.42	10.16	-21.13
685	SA	st?	2.8	63.3	0.816	0.043	1.783	0.071	62.1	12.73	0.22	9.66	0.34	9.65	-18.96
686	SB	sy2	1.7	58.9	1.084	0.110	2.292	0.046	59.3	9.67	0.12	9.17	0.30	9.63	-20.34
688	SA	st?	2.0	49.5	0.733	0.085	2.168	0.057	144.7	12.04	0.64	10.36	0.16	10.30	-20.69
691	SB	stb	5.1	59.4	1.208	0.043	1.954	0.044	46.2	10.42	1.50	9.91	0.22	10.12	-20.72
701	SA	st?	1.1	39.3	1.063	0.051	2.134	0.141	70.7	11.24		9.57	0.10	9.99	-19.75
703	SB	stb	2.1	40.6	1.310	0.061	1.890	0.158	51.0	9.51		10.01	0.11	10.19	-20.57
708	SB	stb	4.1	74.4	1.341	0.039	2.052	0.015	27.1	9.68	1.48	9.15	0.30	9.76	-18.95
710	SB	stb	2.5	55.4	1.341	0.032	2.030	0.034	20.2	9.96	1.24	9.13	0.12	9.20	-18.21
712	SB	stb	3.6	62.9	1.036	0.070	2.169	0.068	61.9	11.82	0.35	9.92	0.15	9.71	-20.70
718	SA	stb	5.4	26.2	0.795	0.051	2.374	0.049	112.1	10.58	2.33	9.79	0.32	10.46	-20.67
721	SA	stb	4.9	38.0	0.720	0.053	2.112	0.103	128.6	11.97	1.40	9.69	0.29	10.24	-20.39
731	SB	stb	-1.3	49.3	1.317	0.073	2.102	0.066	19.4	9.70	1.94	8.31	0.27	9.21	-17.79
739	SA	sy1	3.8	33.7	0.789	0.080	2.429	0.187	120.3	10.45	0.57	9.41	0.30	10.49	-21.17
752	SB	stb	4.1	37.1	0.971	0.056	2.017	0.083	82.0	11.70	0.44	9.86	0.23	9.90	-20.38
759	SB	stb	5.2	40.0	1.271	0.128	2.173	0.057	30.2	9.63		9.70	0.20	9.81	-19.94
769	SA	stb	1.0	65.7	1.302	0.077	1.999	0.025	24.2	9.49	0.30	9.72	0.33	9.85	-19.80
781	SB	stb	4.6	41.6	1.305	0.059	2.161	0.078	38.9	9.87	0.49	9.51	0.20	9.68	-20.15
785	SA	st?	1.3	42.2	0.628	0.094	2.304	0.095	198.8	11.64		10.12	0.48	10.72	-22.25
799	SB	stb	3.1	51.6	1.337	0.043	2.290	0.044	43.2	8.98	2.27	9.59	0.18	10.48	-20.86
804	SB	stb	4.9	33.4	0.813	0.073	2.291	0.068	73.1	13.04	0.31	9.38	0.31	9.76	-19.97
809	SA	stb	5.3	59.5	0.982	0.126	1.795	0.037	104.0			9.96	0.30	10.48	-20.57
814	SB	stb	3.2	56.9	1.018	0.288	2.279	0.076	54.7	10.38	0.38	9.76	0.19	9.84	-18.75
827	SA	st?	4.1	74.0	1.042	0.040	2.210	0.041	75.9	11.21		10.20	0.13	10.01	-20.57
834	SA	st?	2.0	27.3	1.021	0.086	2.508	0.052	147.4	10.50		10.30	0.25	10.94	-21.81
839	SA	st?	1.7	48.2	1.232	0.116	1.851	0.104	55.6	10.50		9.79	0.40	10.36	-21.12
851	SA	sy?	1.7	18.1	0.969	0.050	2.438	0.040	144.7	11.82		9.65	0.43	10.46	-20.90
853	SA	st?	4.9	0.0	0.954	0.107			84.4	11.62		9.76	0.30	10.08	-20.62
860	SB	stb	3.4	61.8	0.645	0.165	1.811	0.129	94.3		0.25	9.50	0.35	10.43	-20.28
861	SB	stb	4.9	20.8	0.756	0.118	2.393	0.047	60.9	10.63		9.36	0.26	9.85	-19.91
871	SB	sy1	5.2	60.3	0.816	0.072	2.424	0.025	137.1	10.90		9.88	0.30	10.31	-21.72
874	SB	stb	3.4	48.4	0.745	0.057	1.977	0.062	59.0	13.20	0.34	9.52	0.18	9.33	-18.69
881	SA	st?	5.5	48.6	0.624	0.094	2.102	0.086	118.9	11.80	1.75	10.05	0.28	10.52	-20.71
898	SB	stb	3.1	54.1	0.987	0.059	2.224	0.065	69.1	10.89	1.78	9.34	0.32	9.78	-19.66
899	SA	sy?	3.8	27.2	0.977	0.046	2.164	0.074	72.7	11.28		9.73	0.28	9.82	-20.47
905	SA	st?	-1.8	53.5	1.071	0.056	1.855	0.058	65.3	10.07		10.00	0.18	9.95	-20.06
906	SA	st?	-0.1	41.3	1.261	0.066	2.264	0.071	86.5	10.07		10.03	0.30	10.32	-20.58
907	SA	st?	7.7	78.8	1.289	0.125	1.891	0.032	18.1	10.25	0.54	8.81	0.16	9.16	-19.54
908	SA	sy?	2.7	61.6	1.177	0.067	1.978	0.034	19.0	10.83		8.87	0.18	8.72	-18.94
910	SA	st?	1.1	38.4	0.916	0.140	2.313	0.065	65.2	10.39		9.29	0.40	9.90	-20.38
917	SB	sy2	1.0	21.5	0.998	0.085	2.458	0.410	99.7	10.54		9.38	0.30	10.74	-21.05
922	SA	st?	4.9	0.0	0.659	0.165			78.4	11.32		9.66	0.31	9.98	-20.30
928	SA	sy2	-0.9	40.0	1.133	0.122	1.823	0.163	97.2	10.75		9.59	0.29	11.01	-20.93
929	SA	st?	3.4	49.5	0.766	0.095	2.232	0.078	72.6	11.26		9.74	0.23	10.04	-20.75
937	SA	sy2	5.3	27.5	0.826	0.048	2.105	0.105	118.0	11.19		9.89	0.28	10.15	-21.06
943	SA	sy?	3.9	60.8	0.693	0.128	2.017	0.152	69.1	11.78		9.31	0.31	9.82	-19.67

Table 9. Integrated quantities for the Mrk IRAS galaxies (*continued*)

Mrk	Bar	Spe	t	incl.	$\log(d_c)$		$\log(V_m)$		D	m_K	O/H	$\log(M_{\text{HI}})$		$\log(L_{\text{FIR}})$	M_B
(1)	(2)	(3)	(4)	[deg]	[0.1']	(7)	(8)	(9)	[Mpc]	[mag]	[\odot]	(13)	(14)	[L_{\odot}]	[mag]
955	SB	sy2	4.2	60.6	0.935	0.064	2.046	0.195	139.0	10.76		9.83	0.53	10.49	-21.21
958	SA		4.0	86.1	1.079	0.046	2.140	0.012	84.8	11.43		9.84	0.30	9.91	-20.64
960	SA	stb	-1.9	71.9	0.900	0.050	1.981	0.060	84.1	11.93	0.30	9.75	0.10	10.14	-20.20
966	SA	st?	0.4	46.9	0.952	0.065	1.971	0.143	70.4	10.83		8.94	0.80	10.09	-19.62
968	SB	stb	4.0	24.1	1.094	0.048	2.256	0.023	58.8	10.17		9.96	0.15	9.65	-20.47
984	SB	lin	7.9	69.8	1.049	0.072	2.284	0.037	190.4	10.59		10.03	0.21	10.58	-22.04
987	SA	st?	4.6	65.9	1.131	0.077	2.281	0.024	66.5	10.39		9.08	0.30	10.15	-20.80
997	SA	sy?	4.2	63.3	1.024	0.040	2.197	0.026	76.3	11.22		10.30	0.08	10.09	-20.41
1002	SA	stb	-1.5	38.6	1.078	0.117	2.183	0.088	41.9	10.10	0.73	9.21	0.23	10.07	-19.47
1003	SA	sy?	2.7	53.1	0.911	0.074	1.946	0.046	48.4	10.90		8.97	0.30	9.36	-19.56
1009	SB	stb	3.1	63.0	1.297	0.188	2.264	0.038	56.8	10.25	0.78	9.86	0.19	9.82	-20.85
1026	SB	stb	2.0	44.8	1.152	0.049	2.221	0.040	51.5	10.46	0.65	9.91	0.12	9.79	-20.29
1027	SA	stb	8.8	45.6	0.844	0.099	2.457	0.056	120.6		0.59	10.03	0.26	11.05	-20.73
1039	SA	stb	5.0	75.2	1.181	0.069	1.860	0.057	26.4	11.84	0.18	9.01	0.16	9.12	-18.64
1043	SA	stb	0.3	48.3	1.143	0.053	1.992	0.110	31.7	10.22	0.91	8.65	0.32	9.39	-19.10
1050	SB	stb	1.1	67.5	1.085	0.073	2.099	0.047	67.0	10.12		9.59	0.11	10.52	-20.54
1063	SA	stb	9.1	70.6	1.265	0.046	1.977	0.032	18.5	10.51	0.27	9.53	0.29	9.18	-19.09
1064	SA	st?	-1.9	38.8	1.060	0.049	2.014	0.040	59.5	10.83		9.89	0.11	10.15	-20.07
1066	SB	sy2	-1.2	68.2	1.214	0.107	1.991	0.255	49.7	9.79	0.25	8.81	0.48	10.53	-19.78
1067	SB	stb	1.7	40.2	1.152	0.058	2.356	0.064	57.5	9.87		9.66	0.10	10.07	-19.98
1068	SA		9.1	90.0	1.123	0.043	2.035	0.027	68.3	11.13		10.26	0.30	9.96	-20.21
1073	SB	sy2	3.1	32.8	1.047	0.049	2.474	0.134	94.9	10.11	0.62	9.60	0.30	11.01	-21.16
1080	SB		8.2	90.0	1.560	0.092	1.879	0.031	10.2	10.37		9.32	0.06	8.43	-19.03
1081	SA	sy?	1.7	20.4	0.976	0.047	2.563	0.023	70.3	10.64		9.83	0.16	9.89	-20.35
1085	SA	st?	4.2	59.2	1.058	0.045	2.224	0.080	65.2	10.45		9.72	0.19	9.89	-20.89
1086	SB	stb	2.7	42.1	0.953	0.045	2.264	0.059	113.2	11.58	0.79	10.11	0.21	10.21	-20.49
1087	SA	stb	-1.8	47.8	1.009	0.066	2.193	0.067	110.2	11.86	0.34	10.22	0.18	10.77	-21.13
1088	SB	stb	0.1	20.7	1.244	0.041	2.654	0.361	60.4	9.20	1.38	9.43	0.22	10.53	-21.63
1089	SA	stb	8.9	64.7	0.930	0.219	1.911	0.089	52.7	11.84	0.39	10.18	0.12	10.19	-18.92
1092	SB	st?	3.1	75.6	1.244	0.078	2.215	0.015	43.0	10.31		9.94	0.06	9.32	-21.20
1093	SA	stb	1.1	47.5	1.076	0.123	2.362	0.082	57.9	10.19	2.05	9.93	0.30	10.63	-20.06
1104	SA	st?	2.1	26.5	0.892	0.082	2.139	0.224	29.8	11.54		9.55	0.30	9.23	-17.56
1116	SA		4.9	36.8	0.968	0.103	2.333	0.062	109.2	10.56		9.88	0.53	10.96	-21.36
1118	SA	st?	3.0	48.6	1.285	0.040	2.360	0.124	44.1	9.65		10.13	0.12	9.75	-20.11
1124	SA	sy?	4.8	39.0	1.134	0.038	2.091	0.058	66.4	11.10		10.00	0.12	9.58	-20.32
1127	SA	stb	3.0	75.8	1.196	0.041	2.324	0.012	101.9	10.49	0.06	10.13	0.30	10.24	-21.19
1137	SA	st?	4.3	28.8	0.866	0.076	2.292	0.160	103.5	11.86		9.89	0.30	10.26	-20.30
1149	SB	stb	5.0	63.0	1.021	0.060	2.166	0.028	82.9	11.61	1.07	9.84	0.18	9.88	-20.53
1157	SB	sy2	-0.1	38.5	1.165	0.064	2.086	0.095	62.3	10.06		9.37	0.28	10.05	-20.33
1171	SA	stb	5.3	49.1	1.214	0.057	1.667	0.115	70.5	9.68	2.40	9.98	0.11	10.29	-21.12
1194	SB	stb	-2.0	53.8	1.246	0.044	2.251	0.044	58.8	9.23		9.46	0.19	10.55	-20.75
1197	SA	sy?	4.2	57.5	0.799	0.049	2.197	0.095	66.7	10.84		9.34	0.30	9.91	-19.63
1198	SA	sy?	3.5	68.8	1.065	0.051	2.414	0.032	102.8	10.26		10.38	0.19	10.28	-21.07
1199	SA	stb	2.7	42.9	1.023	0.076	1.859	0.196	55.0	10.16	1.14	9.10	0.38	10.45	-20.79
1200	SB	stb	2.7	26.4	0.962	0.107	2.486	0.022	104.7	10.35		10.06	0.17	10.39	-20.85
1225	SA	sy?	2.3	66.5	1.042	0.170	2.264	0.020	50.9	10.92		9.56	0.30	9.14	-19.31
1233	SA	st?	3.6	57.5	0.839	0.053	2.172	0.058	64.6	11.18		9.77	0.27	10.24	-19.18
1235	SA	st?	5.0	52.5	1.122	0.045	1.989	0.100	65.1	10.37		9.67	0.10	9.90	-20.94
1270	SA	sy?	5.0	43.8	1.086	0.050	2.250	0.066	110.7	11.70		10.34	0.19	10.24	-20.84
1273	SB	stb	0.0	54.9	0.851	0.061	2.234	0.243	110.1	11.37		9.57	0.55	10.13	-20.33
1291	SB	sy2	3.9	33.2	1.436	0.039	2.367	0.097	48.5	9.52		10.09	0.10	9.89	-21.14
1302	SB	stb	3.0	62.5	1.003	0.055	1.710	0.032	74.7	10.94	0.90	9.96	0.10	9.68	-19.54
1304	SA	stb	3.0	57.6	1.053	0.195	2.137	0.083	73.4	11.34	0.53	9.75	0.30	10.43	-20.16
1326	SB	stb	5.9	28.9	1.217	0.031	2.114	0.107	19.4	10.96	1.68	8.64	0.20	8.85	-18.56
1330	SB	sy1	3.0	54.9	1.475	0.094	2.313	0.091	33.3	8.11		9.34	0.15	9.71	-20.31
1333	SA	sy2	2.9	78.3	1.216	0.051	2.306	0.015	37.7	9.46		9.47	0.10	9.83	-19.54
1337	SA	st?	2.1	54.3	1.113	0.056	2.160	0.029	34.4	10.50		9.34	0.13	9.76	-18.89
1341	SB	stb	5.9	50.6	1.330	0.037	2.087	0.052	16.2	10.29	0.85	9.01	0.36	9.07	-18.69
1344	SB	stb	-2.0	30.8	0.978	0.050	2.116	0.045	42.2	10.37	0.28	9.44	0.15	9.80	-18.72
1346	SB	stb	6.5	75.8	1.217	0.030	1.831	0.024	15.4	11.92	0.20	9.00	0.09	8.51	-17.74
1356	SA		1.7	45.3	0.842	0.056	1.894	0.266	159.1	11.11		9.68	0.75	10.50	-21.07
1363	SB	stb	1.1	34.3	1.278	0.049	2.236	0.015	36.7	9.70		9.48	0.12	9.46	-20.38
1365	SB	stb	-2.0	44.8	0.985	0.107	2.101	0.109	75.5	10.32	0.42	9.27	0.30	10.50	-19.71
1379	SB	stb	2.2	33.6	1.152	0.079	1.821	0.153	35.5	9.63	1.45	9.45	0.10	9.93	-19.99
1381	SA	st?	4.0	75.1	1.030	0.047	2.281	0.012	109.5	11.62		9.91	0.21	10.24	-20.49
1403	SA	sy1	4.8	53.4	0.740	0.045	2.006	0.091	112.8	12.44		9.88	0.29	10.12	-19.86
1425	SA	st?	4.5	60.5	0.964	0.067	2.176	0.039	101.6	10.85		10.11	0.19	10.24	-20.77
1452	SB	stb	4.9	40.9	0.796	0.072	2.087	0.082	92.1	11.54	1.07	9.92	0.22	9.85	-19.85
1461	SA	sy?	3.5	52.2	0.751	0.071	1.985	0.040	86.8	12.56		9.38	0.27	9.90	-19.96
1466	SB	stb	5.0	47.5	1.613	0.065	2.127	0.073	18.2	8.79	1.48	9.67	0.13	9.48	-19.55
1485	SB	stb	3.6	45.0	1.430	0.144	2.282	0.078	33.9	8.62	2.12	9.90	0.13	9.76	-20.74